Charles University

Faculty of Science

Study program: Chemistry

Study branch: Chemistry

Adam Hegedüš

Tin in hydrogenation catalysis

Cín v hydrogenační katalýze

Bachelor's thesis

Supervisor: Martin Hulla, Ph.D.

Prague 2025

Vyhlásenie

Vyhlasujem, že som záverečnú prácu spracoval samostatne, a že som uviedol všetky použité informačné zdroje a literatúru. Tato práca ani jej podstatná časť neboli použité k získaniu iného alebo rovnakého akademického titulu.

V Prahe 16. mája 2025

Declaration

I hereby declare that I have written this thesis independently and all sources are listed in the bibliography. Furthermore, this work, nor its significant part was used to claim other, or the same academic title.

In Prague 16 May 2025

Adam Hegedüš

Acknowledgements

I would like to thank my supervisor Martin Hulla, Ph.D. for the given opportunity to work on my thesis in his research group and for his supervision over the project. He has my respect and thankfulness for all the skills and knowledge he shared with me. I would like to thank Mgr. Martin Zábranský, Ph.D. for his willingness to teach me almost everything I know about crystallography. Furthermore, I would like to thank my family, friends and everyone who supported me during my studies.

Abstract

This thesis investigates hexa-coordinated tin(IV) and tetra-coordinated tin(II) complexes as imine hydrogenation catalysts with molecular hydrogen as the reducing agent. Steric hindrance around the complexes prevents formation of a classical Lewis acid-base adduct between the Lewis acidic complexes and the imine substrate, leading to the formation of frustrated Lewis pairs (FLP). FLPs possess the unquenched reactivity of the Lewis acid and Lewis base and are capable of molecular hydrogen activation. Two factors affect FLPs' reactivity. First, highly acidic metal center with high hydride ion affinity may facilitate H_2 activation but may also bind the reaction products, and hence slow down the reaction. Second, ligand size controls the Lewis acid's steric hindrance. Too small ligands allow classical Lewis adduct formation, while too big ligands prevent substrate approach to the Lewis acid, and hence its reduction. This thesis focuses on Sn-based Lewis acids for FLP chemistry using modified tetradentate Schiff base ligands to improve the solubility of the complexes in non-polar media, and to reach appropriate steric hindrance. Mono-tert-butyl substituted complexes yield the imine hydrogenation product in 90 % yield, whereas with the di-tert-butyl substituted complexes the yield is 0 %. Various combinations of axially bound ligands are tested to influence the electronic and steric properties of the final complexes.

Keywords

Tin, catalysis, main group chemistry, Lewis acid

Abstrakt

Táto práca skúma hexa-koordinované komplexy cínu(IV) a tetra-koordinované komplexy cínu(II) ako imínové hydrogenačné katalyzátory s molekulárnym vodíkom ako redukčným činidlom. Stérická nedostupnosť okolo komplexov bráni tvorbe klasického Lewisovho acido-bázického aduktu medzi Lewisovými kyslými komplexmi a imínovým substrátom, čo vedie k tvorbe frustrovaných Lewisových párov (FLP). FLP majú nepotlačenú reaktivitu Lewisovej kyseliny a Lewisovej zásady a sú schopné aktivácie molekulárneho vodíka. Reaktivitu FLP ovplyvňujú dva faktory. Po prvé, vysoko kyslé kovové centrum s vysokou afinitou k hydridovým iónom môže uľahčiť aktiváciu H_2, ale môže tiež viazať reakčné produkty, a teda spomaliť reakciu. Po druhé, veľkosť ligandu riadi stérickú nedostupnosť Lewisovej kyseliny. Príliš malé ligandy umožňujú tvorbu klasického Lewisovho aduktu, zatiaľ čo príliš veľké ligandy bránia prístupu substrátu k Lewisovej kyseline, a teda jej redukcii. Táto práca sa zameriava na Lewisove kyseliny pre FLP na báze Sn využívajúce modifikované tetradentátne ligandy Schiffovej bázy na zlepšenie rozpustnosti komplexov v nepolárnych rozpúšťadlách a na dosiahnutie vhodnej stérickej nedostupnosti. Mono-terc-butyl substituované komplexy poskytujú produkt hydrogenácie imínu v 90 % výťažku, zatiaľ čo s di-terc-butyl substituovanými komplexmi je výťažok 0 %. Na ovplyvnenie elektrónových a stérických vlastností konečných komplexov sa testujú rôzne kombinácie axiálne viazaných ligandov.

Kľúčové slová

Cín, katalýza, prvky hlavných skupín, Lewisova kyselina

Contents

List of abbreviations and symbols

LA – Lewis acid

LB – Lewis base

HOMO – highest occupied molecular orbital

FLP – Frustrated Lewis pair

LUMO – lowest unoccupied molecular orbital

TM – Transition metal

R_3Sn^+ - alkyl stannylium ion

Ar_3B – triaryl borane

EtOH – ethanol

$SnCl_4$ – tin(IV) chloride

DCM – dichloromethane

Et_3N – trimethylamine

AgOTf – silver triflate

eq. – equivalent

AgCl – silver chloride

$SnCl_2$ – tin(II) chloride

THF – tetrahydrofuran

sXRD – single-crystal X-ray diffraction

1. Introduction

1.1 Frustrated Lewis pairs

According to the Lewis acid-base theory, any atomic group, molecule or ion capable of accepting electron pairs is classified as an acid, while those that can donate electron pairs are classified as bases. These are usually referred to as Lewis acids (LAs) and Lewis bases (LBs).[1,2] A classical Lewis adduct forms by datively bonding the LA and the LB together, thus providing stabilization with a lower energy of the highest occupied molecular orbital (HOMO) (Figure 1a), quenching the LA's and LB's reactivity. A Frustrated Lewis pair (FLP) forms by combining the LA and the LB, with enough steric bulk so they cannot form the classical Lewis adduct. Suppressing the adduct formation allows for the lowest unoccupied molecular orbital (LUMO) of the LA and HOMO of the LB to react in a non-classical way, forming the FLP (Figure 1b). The FLP therefore contains both Lewis acidic and basic orbitals respectively, that have been shown to activate small molecules such as dihydrogen (vide infra).[3,4]

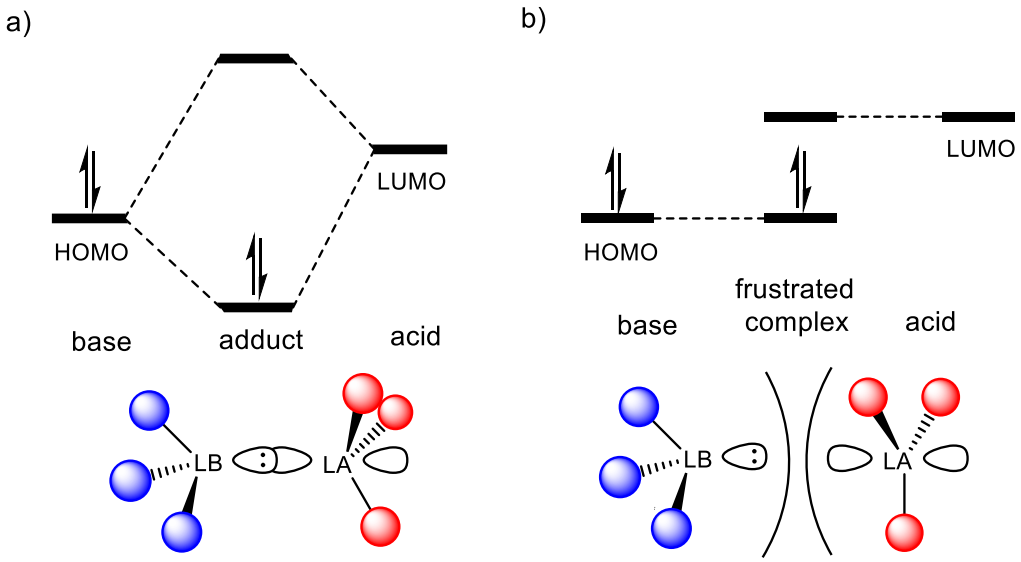

Figure 1: A molecular orbital depiction of formation of a classical Lewis adduct (a) and a frustrated Lewis pair (b).

FLPs can be divided into intra- or inter-molecular. Intra-molecular means that both LA and LB sites are on the same molecule. Intra-molecular FLPs allow for the controlling of the distance between LA and LB sites respectively. The control over geometry can be

applied to optimize the interaction with different moieties present in the solution. Inter-molecular means that LA and LB sites each reside on different molecules, making them require bulkier substituents in order to achieve the desired reactivity. Synthetically, it is easier to tune their reactivity than in intra-molecular FLPs, although, it is more difficult in practice to desirably prepare inter-molecular FLPs. However, spatial strain is not the only parameter influencing reactivity. The cumulative acidity and basicity also plays a crucial role on the character of the interaction. [5,6]

The common examples of Lewis acids used in FLP chemistry are compounds of group 13 and 14 metals and semi-metals. The most common are B, Al, Ga and Si, Ge, Sn LAs. Both cationic and neutral LAs have been prepared. Boranes, silanes and triaryl-aluminum LAs are common examples of neutral LAs. Borenium cations and trivalent silylium cations are common examples of cationic LAs.[4,7] The positive charge of the cationic LAs makes them highly electrophilic, hence allowing easier small molecule activation and dihydrogen splitting (vide infra). Nonetheless, the positive charge also makes them more susceptible to quenching by hydroxylic species.[8–10]

The Lewis acidity of the respective cation can be regulated by the type of ligands, which the cation bonds to. The resulting change in electrophilicity of the cation can then influence how the complex moiety interacts with the rest of the system in question.[10,11] Another factor to keep in mind is the ligand size. The ligands surrounding the central atom have to be bulky enough to prevent adduct formation, while not being too bulky in order to achieve reactivity.

The first to prepare FLPs capable of dihydrogen activation were Stephan and co-workers in 2006. They observed a heterolytic cleavage of H_2 molecule in the presence of a bulky phosphine-borane system.[12] However, boron based FLPs suffer from low tolerance to hydroxylic species, with which they form strong Brønsted acidic adducts. These adducts are then easily deprotonated, leading to the FLP deactivation. Low thermal stability adds to this, as with increasing temperature, it becomes easier to decompose the boron based LAs. This moisture intolerance has been partially overcome by using weak bases such as THF or 1,4-dioxane, bases that deprotonate the LA-OH_2 adduct reversibly.[13]

To resolve the moisture intolerance, Sn based FLPs were developed. Notably, the $^{i}Pr_3SnOTf$ LA showed higher tolerance to hydroxylic species and better thermal stability than the boron based systems. The pK_A of $[^{n}Bu_3Sn\text{-}OH_2]^+$ = 6,25 in water, whereas the pK_A of $H_2O\text{-}B(C_6F_5)_3$ is lower than 1. Yet, $^{n}Bu_3Sn\text{-}H$ has a $\Delta G_{hydride}$ = 65.8 kcal · mol^{-1}, which

is similar to that of $HB(C_6F_5)_3$ ($\Delta G_{hydride}$ = 64.95 kcal · mol^{-1}). Therefore, the corresponding LAs favor dihydrogen activation equally and the hydrides act as comparable reducing agents. As a result, soft stanylium ions are more water tolerant without affecting the dihydrogen activation and hydrogenation activity. The Sn based species also showed high versatility in substrate scope, as they were able to catalyze hydrogenation of various unsaturated functional groups such as imines, alkenes and carbonyls.[14–17]

1.2 Hydrogenation reactions

Hydrogenations of unsaturated bonds, such as imines, alkenes, alkynes, aldehydes and ketones, belong to some of the most important industrial processes. These hydrogenations are usually catalyzed by transition metal (TM) systems, ranging from heterogeneous zeolites to highly selective homogeneous complexes of Pd, Pt, Rh, Ir. Such catalysts can be considered as an integral part of pharmaceutical as well as petrochemical industries respectively. Splitting of H_2 by a TM results from the interaction of a vacant orbital of the TM and a σ-bonding orbital of the H_2. Single-site TM systems usually achieve H_2 activation by one of three mechanisms. Either by (1) oxidative addition, (2) by σ-bond metathesis or (3) by base assisted heterolytic cleavage (Scheme 1). The oxidative addition mechanism usually occurs in low-valent TMs. It commences with the coordination of H_2 forming a dihydrogen complex via a dative bond. Such intermediate then undergoes oxidative addition, facilitated by the d → σ^* back donation, resulting in the formation of a dihydride moiety (Scheme 1a). Subsequently, the substrate binds to the metal center for the hydride insertion to the substrate. Finally, reductive elimination of the reduced substrate produces the hydrogenated product and regenerates the catalyst.[18,19]

Conceptually, σ-bond metathesis is an exchange of a M-L σ-bond with σ-bond of H_2 or substrate and usually occurs in high-valent TMs. The reaction cycle is usually initiated by generation of a metal hydride from precursor catalyst and H_2 by σ-bond metathesis (Scheme 1b). The insertion of an unsaturated substrate causes a cycloaddition reaction through a four-centered transition state by exchange of ligands. The saturated ligated product then participates in further σ-bond metathesis with H_2 to yield the desired product, regenerate the TM-hydride and restart the reaction cycle again.[20–23]

The LB-TM cooperation mechanism initiates with the TM binding H_2 to create TM-H_2. This step is then followed by deprotonation of the TM-H_2 with LB, by providing electron density to the σ^* orbital of the H_2 to make TM-H and LB-H (Scheme 1c).[18,24]

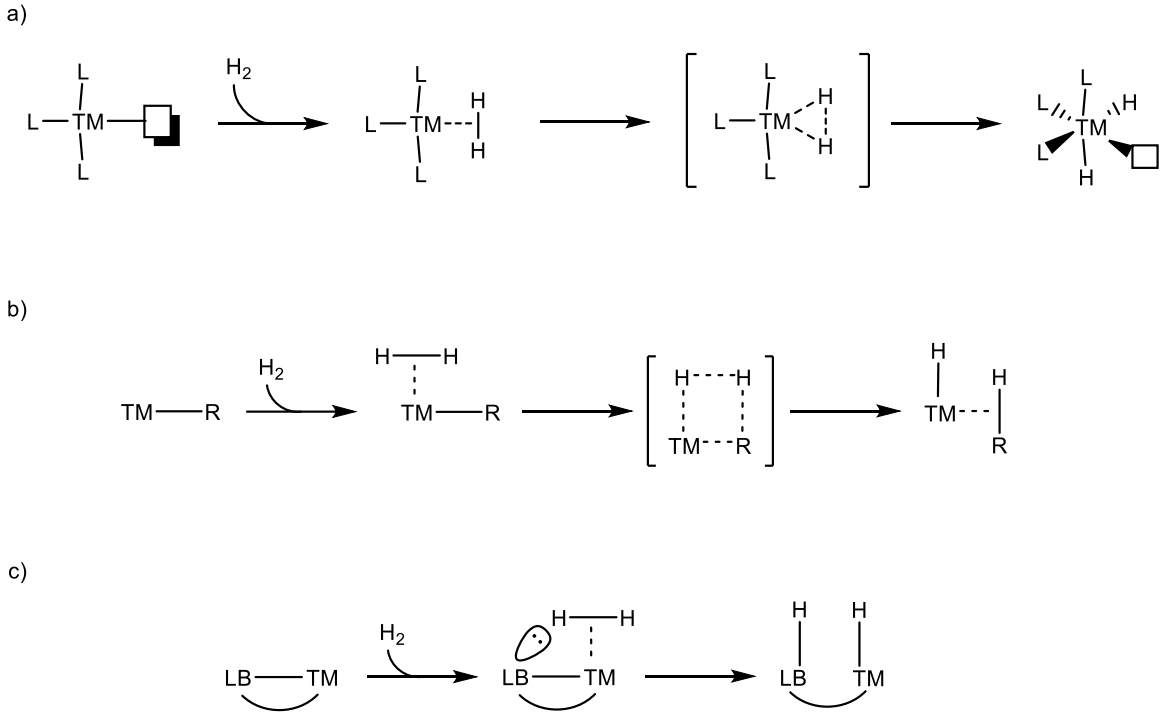

Scheme 1: A general mechanism of single-site transition metal mediated hydrogen activation by either (a) an oxidative addition, (b) σ-bond metathesis and (c) LB-TM cooperation mechanism.

However, commonly used platinum group TM catalysts have disadvantages. For example, their high cost, toxicity and low earth abundance stipulate a need to design sustainable, cheap, earth abundant catalysts that work under ambient conditions. This leads to the study of more abundant first row TMs like Fe, Co, Ni, and even main group elements, such as B, Al, Si, Sn and more.[25,26]

The complementary acidic and basic orbitals of an FLP can activate small molecules such as H_2, and therefore catalyze hydrogenations of various unsaturated bonds. The activation of H_2 occurs through a single transition state via simultaneous electron transfer processes, characterized by concerted action of LA and LB. Electrons are transferred from the LB to the σ^* orbital of H_2 and from σ orbital of H_2 to the LA. Such an interaction leads to the polarization of the H-H bond, which eventually cleaves. This model proposes that LA

and LB sites pre-organize into an energetically strained complex, serving as a highly reactive species for bond activation (Scheme 2).[27,28]

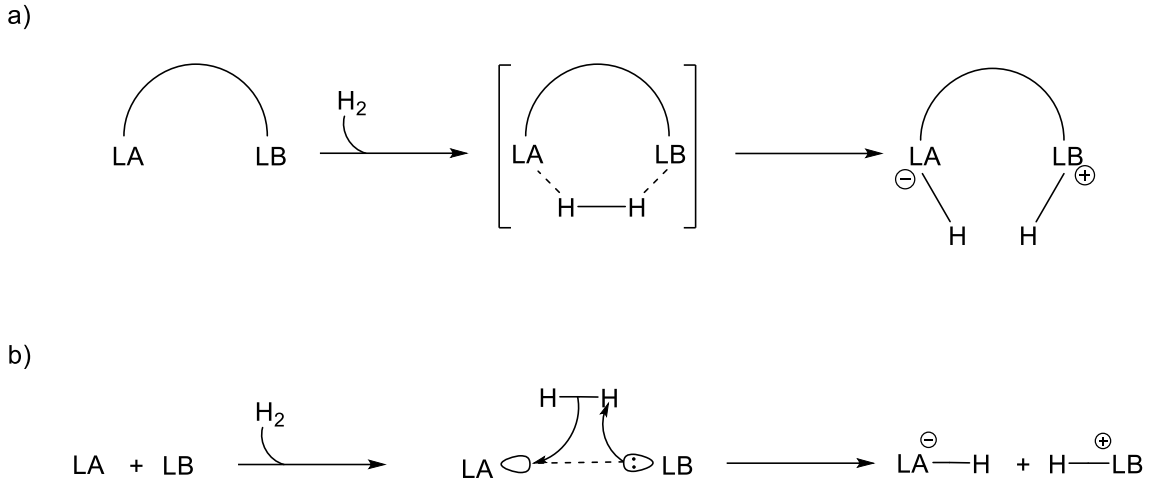

Scheme 2: A general mechanism for activation of hydrogen by an intra-molecular frustrated Lewis pair (a) and by an inter-molecular frustrated Lewis pair (b).

Subsequent protonation of substrate by LB-H can easily occur. This step is then followed by hydride transfer from LA-H, which acts as the hydride source, reducing the activated substrate. The FLP is therefore regenerated and can participate in the next reaction cycle (Scheme 3).

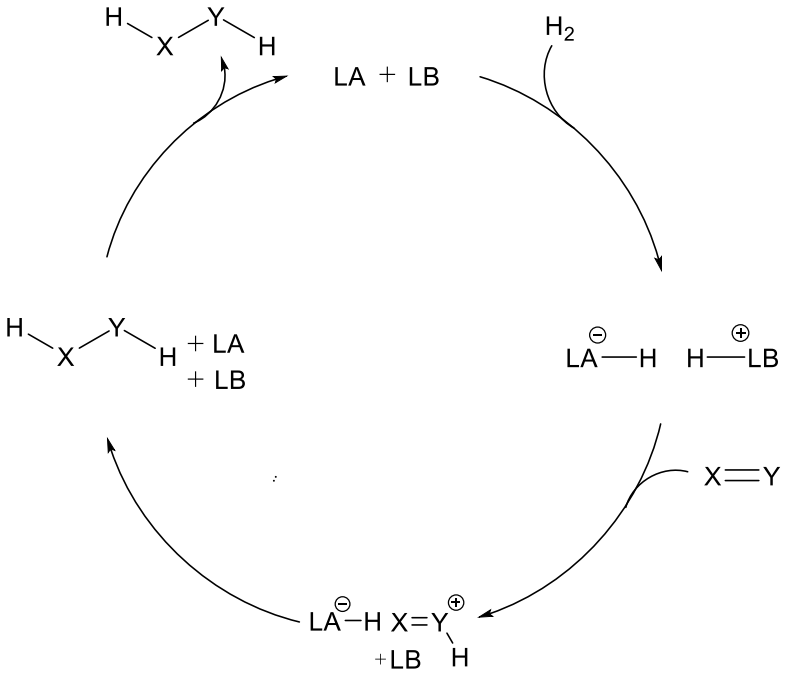

Scheme 3: A mechanism of hydrogenation of an unsaturated substrate X=Y by a frustrated Lewis pair.

If either the Lewis acidic or the Lewis basic component of the pair is too strong, the catalytic activity decreases due to slow or incomplete protonation of the substrate, or due to high affinity and binding of the substrate or product to the LA component of the FLP. If, however, the FLP's components are too weak, the rate limiting step is the activation of dihydrogen. Hence, it is apparent that cumulative strength of LA/LB pair determines the catalytic activity, and appropriate tuning of each of the components is necessary to achieve the desired reactivity.[26,29]

In the case, where substrates and/or products of the hydrogenation are LBs, it may be possible to achieve a Lewis acid-only catalysis, where substrates such as imines, are strong enough bases to act as the FLP's basic component in hydrogenation reactions. From mechanistic point of view, the splitting of H_2 is achieved by an LA-imine system yielding an iminium ion and a LA-H^- ion. The protonated imine becomes susceptible to a nucleophilic attack at the iminium carbon by the LA-H^- ion, resulting in the formation of an LA-amine adduct. Dissociation of this adduct creates the corresponding amine and regenerates the LA, which can then participate in the next catalytic cycle (Scheme 4).[30,31]

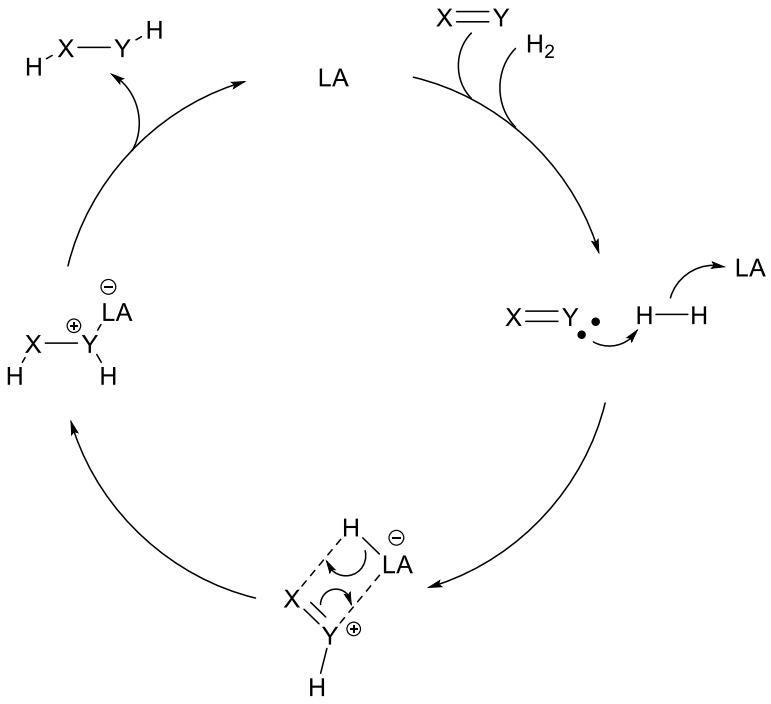

Scheme 4: Lewis acid-only frustrated Lewis pair hydrogenation of an unsaturated substrate.

Imines have been hydrogenated by a range of non-TM catalysts. While boron-based FLPs have been predominantly employed, catalytic systems featuring other cationic centers have been prepared. Mainly Al and Sn-based LAs for FLPs have shown catalytic activity towards hydrogenation of imines.[4,32–34]

1.3 Tin based FLPs

Tin based FLPs were first developed because of their lower oxophilicity and therefore better stability towards hydroxylic species than boron based FLPs. As mentioned, the first example of a tin based FLP is the tetrahedral $^{i}Pr_3SnOTf$ LA in conjunction with N-centered LBs. Trialkyl stannylium (R_3Sn^+) ions are isolobal with the triaryl boranes (Ar_3B) frequently used in FLP catalysis. According to calculations, the R_3Sn^+ species bear similar hydride ion affinities to the Ar_3B species.[14] The computational studies also suggest similar reactivities of R_3Sn^+ species towards hydrogenation of various unsaturated substrates, while retaining lower oxophilicity than the boron species. Furthermore, they showed appreciable moisture and hydroxyl group tolerance in technical grade solvents and reagents without the need for anhydrous conditions. Moreover, the R_3Sn^+ based FLPs display tolerance to elevated temperatures of up to 180 °C as well as tolerance to strong amine bases, whereas boranes usually decompose at temperatures around 120 °C. R_3SnX based FLPs have shown to successfully catalyze reductive coupling of aryl and alkyl amine substrates with CO_2 and H_2, as well as hydrogenations of imines, aldehydes, ketones and alkenes. Also, the amine products of imine hydrogenations act cooperatively with the tin catalyst to enable better H_2 activation. Notably, the lower steric profile of such catalysts even allows to catalyze reductions of bulkier substrates.[14,17,35]

However, in addition to tetravalent compounds, tin also forms octahedral complexes. The first hexa-coordinated complexes using tetradentate Schiff base ligands and two axially bound halide ions of the form L_4SnX_2 for H_2 activation were reported in 2024[36]. Schiff base ligands such as salen (N, N-bis(salicylidene)ethylenediamine) are cheap and well characterized compounds,[37] which can support various tin oxidation states.[38] Unlike purely – alkyl and –aryl substituted tetravalent tin LAs, which offer limited substrate scope for steric hindrance and electronic optimization of the LAs, and are poorly soluble in organic non-polar solvents, substituents of Schiff base ligands can be tuned in order to affect the

solubility, Lewis acidity and steric bulk of the whole complex.[36] However, current understanding of hexa-coordinated tin LAs for hydrogenation catalysis is limited and numerous questions remain unanswered such as: why is the hydrogenation activity of the complexes limited to temperatures above 150°C, while H_2 activation takes place at 25 °C, or what is the effect of the axial ligands beyond their function as leaving groups to open a vacant coordination site for H_2 activation ?

2. Goals of this thesis

The goal of this thesis is to synthesize various hexa-coordinated tin(IV) and tetra-coordinated tin(II) based complexes as Lewis acids for Frustrated Lewis pair catalysis. These complexes are prepared by using Schiff base ligands modified with *para*-^{t}Bu groups to either improve the solubility of the parent tin Salen complex [Sn (*N, N*-bis(salicylidene)ethylenediamine) Cl_2], or avoid excessive steric hindrance in catalytic reactions proposed to limit the reactivity of the 3,5-di-^{t}Bu substituted complex [Sn (*N, N*-bis(3,5-di-tert-butyl-salicylidene) ethylenediamine) Cl_2]. Tin(II) complexes are prepared to decrease the acidity and facilitate easier product release from the metal center, which is a possible limiting factor. Axial coordination sites of complexes are modified with better leaving groups to facilitate creating a vacant coordination site at lower temperatures.

Complexes with such modified ligands are tested in hydrogenation reactions of imines to compare their activity with the ones previously prepared. In addition, complexes of tin(IV) Salens are tested for their affinity to the amine product in catalytic reactions based on the hypothesis, that the dissociation of the amine product from the metal center may be the rate limiting step in this catalysis.

3. Results and discussion

3.1 Synthesis of ligands

The salen, 3-tert-butyl-salen and 3,5-di-tert-butyl-salen ligands (Figure 2) were all prepared according to the literature.[39] The corresponding salicylaldehyde and ethylenediamine were refluxed in ethanol (EtOH) for 2 hours. The resulting product was crystallized by cooling the reaction mixtures at −20°C overnight, filtered and washed with cold EtOH. The products were collected as yellow crystals, flakes or powder.

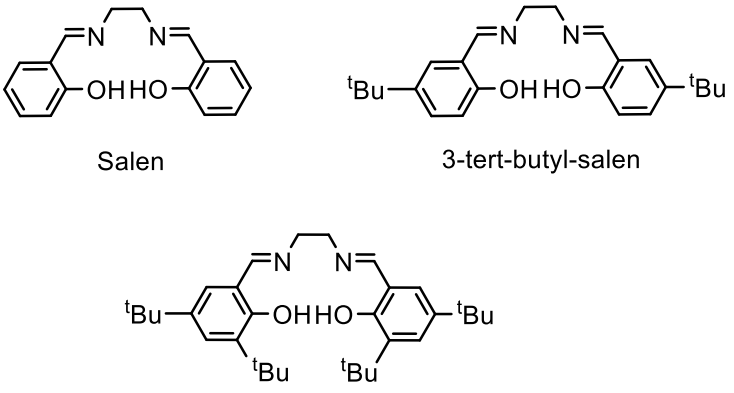

Figure 2: Structures of synthesized ligands.

3.2 Synthesis of complexes

Complexes **1**, **2** and **3** (Scheme 5), were prepared by procedures adapted from the literature.[36] Unless otherwise specified, the syntheses were performed in nitrogen atmosphere using a Schlenk line apparatus due to poor hydrolytic stability of tin(IV) chloride ($SnCl_4$) and or the resulting products. All glassware was dried in the oven overnight prior to use and dry solvents from purifier were used for the syntheses.

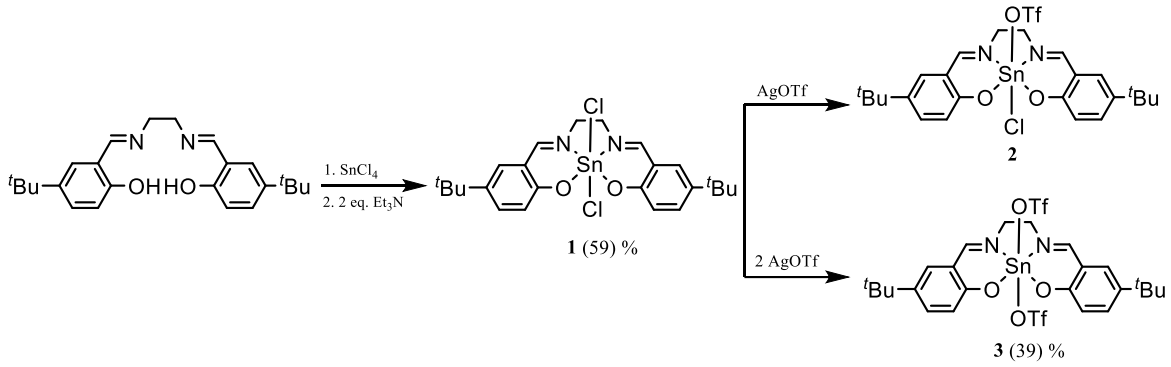

Scheme 5: Structures and reaction pathways for the syntheses of [Sn(3-^{t}Bu-salen)Cl_2], [Sn(3-^{t}Bu-salen)(OTf)Cl] and [Sn(3-^{t}Bu-salen)$(OTf)_2$].

3.2.2 [Sn(3-^{t}Bu-salen)Cl_2] complex **1**

The ligand was dried in vacuum for 1 hour. The ligand was then dissolved in dichloromethane (DCM) and $SnCl_4$ was added and stirred for 5 minutes. Triethylamine (Et_3N) was then added as the ancillary base to help deprotonate the phenolic hydroxyls and to form a chloride salt during the synthesis. The Et_3N was added later because the amine otherwise coordinates to the tin source, hindering the desired reaction. The dichloro complex is stable in air so the reaction work-up under inert atmosphere was not necessary. The work up comprised of evaporating the DCM solvent, washing the solid product with EtOH to purify the product from the ammonium salt and then filtering through a filter paper (repeated three times). The solid was then washed with boiling heptane and filtered through a filter paper while hot to purify the product from the remaining unreacted ligand (repeated twice). The yellow product was then dried in vacuum. The course of the reaction was monitored through NMR measurements. The coupling constant $J_{Sn\text{-}H}$ = 86.16 Hz for complex **1** confirmed the presence of the tin metal in the ligand by its coupling to the –CH=N-R imine function of the ligand. These coupling constants were the initial proof that complexation took place in all syntheses.

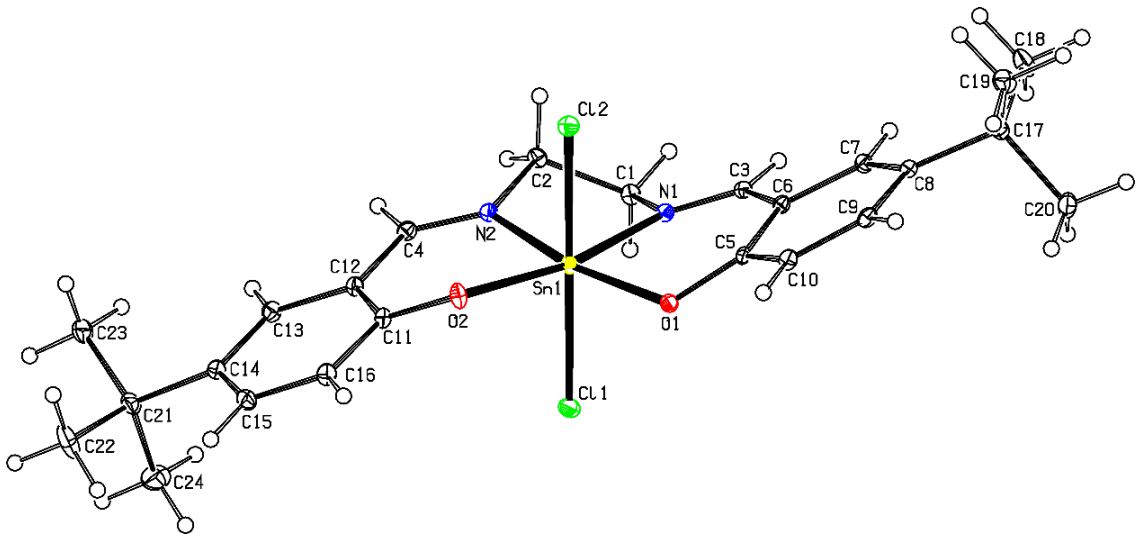

Figure 3: The molecular structure of the complex **1** with the corresponding atom numbering scheme. Thermal displacement elipsoids were plotted at the 30 % probability level. Applied colours: C – black, H – black contour, Cl – green, N – blue, O – red, Sn – yellow.

Crystals of [Sn(3-^{t}Bu-salen)Cl_2] suitable for X-ray diffraction (Figure 3) were obtained by diffusion of excess liquid hexane into a DCM solution of the complex **1**. Complex **1** crystallized in a monoclinic unit cell with a $P2_1/c$ space group and four stannic complex molecules in the unit cell (Figure 4). The deformed octahedral coordination environment enveloping the tin(IV) atom in this complex is analogous to the environment reported for similar compounds described in the literature.[40] Valence angles between N1-Sn1-O1 = 88.53(6)°, N2-Sn1-O2 = 88.57(6)°, O1-Sn1-O2 = 105.95(6)° and N1-Sn1-N2 = 76.96°. Valence angle between Cl1-Sn1-Cl2 = 175.68(2)°. Particularly the fact that Cl1-Sn1-Cl2 angle is not 180° and that O1-Sn1-O2 angle is around 20° larger than N1-Sn1-N2 angle confirms that **1** has a distorted octahedral shape. Torsion angle of N1-C1-C2-N2 = −45.71(19)°. This torsion angle confirms that one phenyl ring lies above the plane of symmetry, while the second phenyl lies below the plane of symmetry, achieving a so called "stepped" conformation, where the five-membered ring is a half-chair similar to an oxomanganese-salen complex reported previously.[41] The distortion of the complex's octahedral geometry is further apparent on the valence angles between Cl1-Sn1-N1 = 93.18(5)° and Cl1-Sn1-N2 = 90.53(5)° as well as Cl2-Sn1-N1 = 90.21(5)° and Cl2-Sn1-N2 = 92.85(5)°. The crystal packing of **1** shows that **1** is racemic with plane of symmetry in O-N-N-O plane (Figure 4). Bond lengths of Sn1-Cl1 = 2.4036(7) Å, Sn1-Cl2 = 2.4250(6) Å, Sn1-O1 = 2.0173(14) Å, Sn1-O2 = 2.0055(14) Å, Sn1-N1 = 2.1525(15) Å and Sn1-N2 =

2.1723(16) Å are similar to other [Sn(Salen)Cl_2] complexes.[36] These bond lengths are however around 0.2 Å shorter than those of tin(II) complex **5** (Figure 5). The shorter bond lengths of **1** in respect to the complex **5** are due to **1** containing a smaller, more charged Sn(IV) cation, that fits better into the O-N-N-O ligand pocket than the larger Sn(II) cation of **5**, which is positioned in a pyramidal position above the plane of the ligand (vide infra). The shorter bond lengths of **1** also shows that the tin(IV) complex **1** binds to oxygen and nitrogen atoms more strongly than the tin(II) in complex **5.**

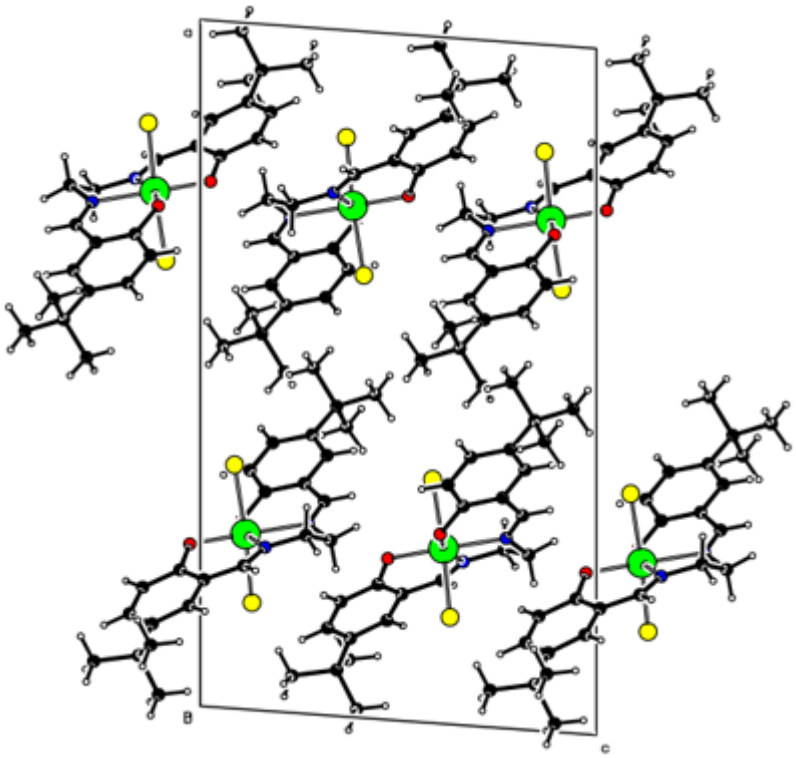

Figure 4: The crystal packing in the structure of **1** viewed along the axis *b*. The unit cell is outlined by a solid line. Applied colours: C – black, H – black contour, Cl – green, N – blue, O – red, Sn – yellow.

3.2.3 [Sn(3-^{t}Bu-salen)(OTf)Cl] complex **2** and [Sn(3-^{t}Bu-salen)$(OTf)_2$] complex **3**

A triflate group is a weakly coordinating anion due to dispersion of the negative charge over 3 oxygen atoms and a CF_3 group. The triflate is thus highly susceptible to substitution by other ligands, and especially by aqua ligands from atmospheric moisture. Hence, all

preparations were made under inert atmosphere using a Schlenk line apparatus. A precursor compound for this synthesis, silver triflate (AgOTf), is also sensitive to light. The Schlenk flasks were therefore wrapped in aluminum foil before starting the procedure, and the AgOTf was handled in a non-illuminated glovebox filled with nitrogen atmosphere. The protocol comprised of drying the starting dichloro complex **1** in vacuum for 1 hour, and then dissolving it in DCM. 1 equivalent (eq.) of AgOTf were added to the solution for synthesis of complex **2** and 2 eq. for complex **3**, and the reaction mixtures were stirred for 96 hours at room temperature. The poorly soluble silver chloride (AgCl) side product allows filtration of the produced complexes in solution via cannula to another flask. The solvent was then evaporated and the yellow products were obtained. For **2** $J_{Sn\text{-}H}$ = 89.96 Hz, while for **3** $J_{Sn\text{-}H}$ = 105.52 Hz around the imine function of the complexes. The $J_{Sn\text{-}H}$ constants are slightly higher for complexes **2** and **3** than complex **1**. This increase clearly shows that the salen ligand donors bind more strongly to the tin center of **2** and **3** as the triflate is a weakly coordinating anion, providing little electron density to the metal center. The tin center thus draws more electron density from the salen ligand, forming stronger bonds. Attempts to crystallize **2** and **3** for single crystal X-ray diffraction (sXRD) were unsuccessful.

3.2.4 [Sn(3-^{t}Bu-salen)] complex **4** and [Sn(3,5-di-^{t}Bu-salen)] complex **5**

The basic protocol was the same for all tin(II) complexes (Scheme 6). Tin(II) chloride ($SnCl_2$) was dried in vacuum at 60 °C for 1 hour. In a separate flask, ligand was dried in vacuum at room temperature for 1 hour. $SnCl_2$ was then dissolved in tetrahydrofuran (THF) and transferred to the flask with the ligand via cannula. Et_3N was then added as an ancillary base to form a chloride salt during the reaction. All the syntheses were performed under an inert atmosphere using Schlenk line apparatus. Glassware was dried in the oven overnight prior to each of the syntheses. Dry solvents were used in all syntheses. The course of the syntheses was monitored through NMR measurements. While the complexes formed, attempts to crystallize complex **4** from $[Et_3NH]Cl$ were unsuccessful due to poor stability of the complex to water and even alcohols that were reported for the purification of related Schiff base complexes of tin(II).[42] The use of alternative bases such as NaH or LiHMDS did not yield the desired complex at all. Complexes **4** and **5** were synthesized by an alternative method. Using $[(Me_3Si)N]_2Sn$ as both the base and the tin source, in dry toluene, yielded the yellow product in case of using both (3-^{t}Bu-salen) (complex **4**) and (3,5-di-^{t}Bu-

salen) (complex **5**) ligands. The coupling constats were $J_{Sn\text{-}H}$ = 23.76 Hz for complex **4** and $J_{Sn\text{-}H}$ = 22.16 Hz for complex **5** around the imine function of the complexes. The $J_{Sn\text{-}H}$ constants are lower for tin(II) complexes than for tin(IV) ones. The smaller charge of tin(II) combined with its bigger size, does not provide as strong bonding and interaction with the salen ligand donors as with the tin(IV) complexes. These strengths of the respective interactions can also be inferred from the bond lengths in sXRD structures.

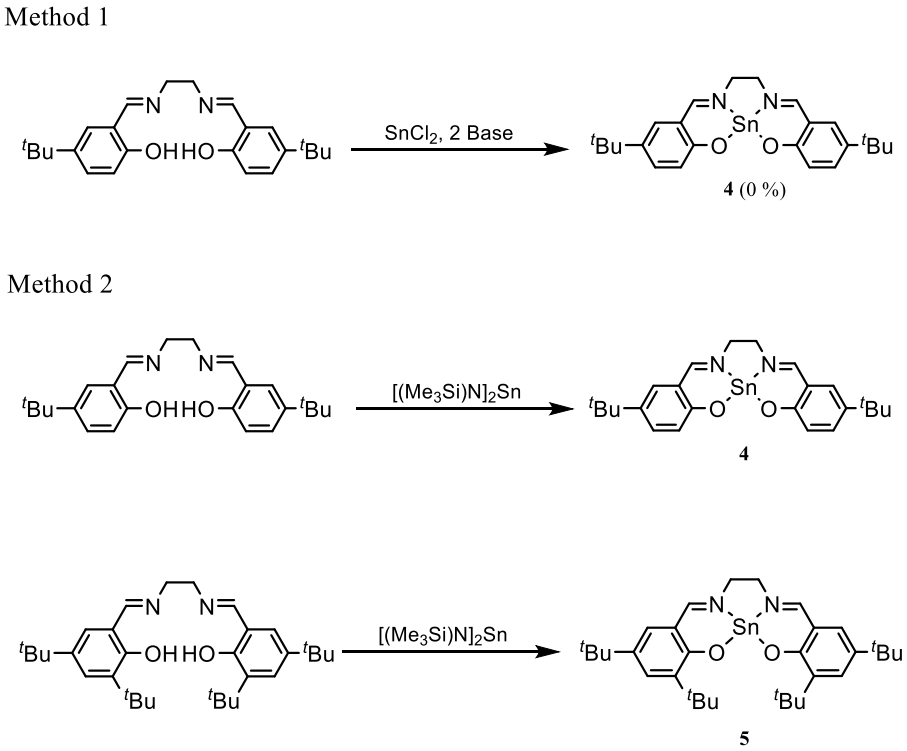

Scheme 6: Synthesis of [Sn(3-tBu-salen)] and [Sn(3,5-di-tBu-salen)].

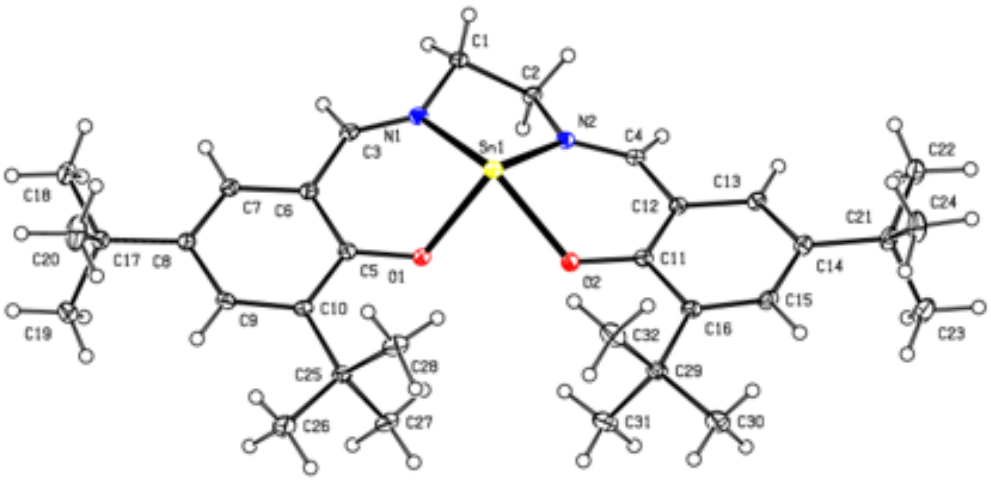

Figure 5: The molecular structure of the complex **5** with the corresponding atom numbering scheme. Thermal displacement elipsoids were plotted at the 30 % probability level. Applied colours: C – black, H – black contour, N – blue, O – red, Sn – yellow.

The investigated crystal of solvated complex **5** (Figure 5) suitable for X-ray diffraction was obtained from a hot heptane solution by cooling during the isolation of **5** from the reaction mixture. [Sn(3,5-di-^{t}Bu-salen)] crystallizes in a monoclinic unit cell with *C*/2*c* space group. Valence angles of O1-Sn1-O2 = 78.91(4)°, N1-Sn-N2 = 68.46(4)°, O1-Sn1-N1 = 75.11(4)° and O2-Sn1-N2 = 77.88(4)° do not support a square planar geometry, which is suggested by the crystal top-view (Figure 5). Moreover, valence angles of O1-Sn1-N2 = 105.17(4)° and O2-Sn1-N1 = 129.51(4)° are far from the ideal 180° of the square planar geometry. The tin(II) center actually lies above the plane of the ligand, engaging in a so called "bowl-shaped" conformation, where the five-membered rings around the tin center adopt an envelope shape (Figure 7). Complexes of tin(II) with similar *N*,*N*′-bis(salicylidene)ethylenediamine-based ligands have been reported to contain the central atom in a deformed tetragonal arrangement of thee donor atoms.[43,44] Accordingly, the central tin(II) atom in the complex **5** is significantly shifted (1.1400(3) Å, Figure 7) out of the mutual plane of the four donor atoms (N1,N2,O1,O2; deviations from the mutual plane smaller than 0.2 Å). The reason for such geometry is that the tin(II) cation is too bulky to fit into the plane of the ligand, as the tin(IV) does, and thus the tin(II) lies above the plane. The crystal packing of **5** (Figure 6) shows that **5** is racemic with plane of symmetry in O-N-N-O plane. The bond lengths of Sn1-O1 = 2.0980(10) Å, Sn1-O2 = 2.1360(11) Å, Sn1-N1 = 2.3776(11) Å and Sn1-N2 = 2.3292 Å are longer than in the tin(IV) analogues as mentioned. These longer bond lengths are indicative of weaker bonding consistent with the lower charge density of the tin(II) cation.

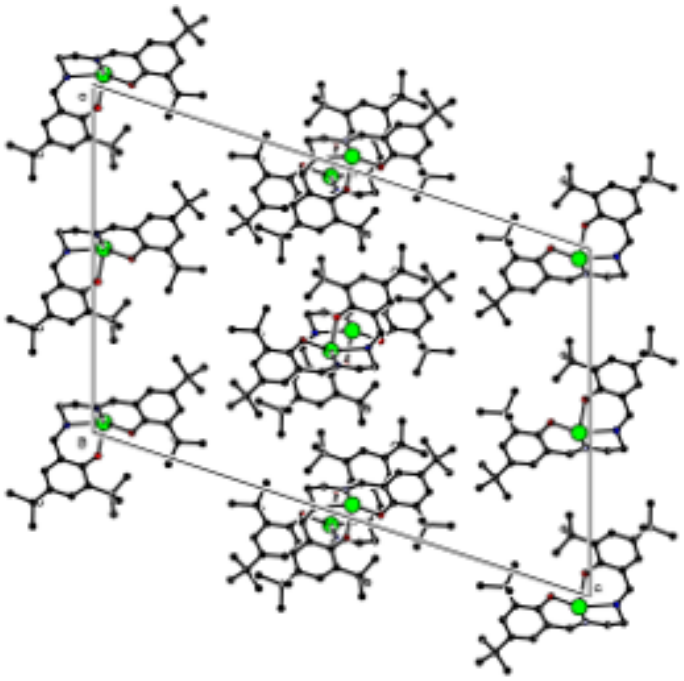

Figure 6: The crystal packing in the structure of **5** viewed along the axis *a*. The unit cell is outlined by a solid line. Hydrogen atoms were omitted from the plot for clarity. Applied colours: C – black, N – blue, O – red, Sn – yellow.

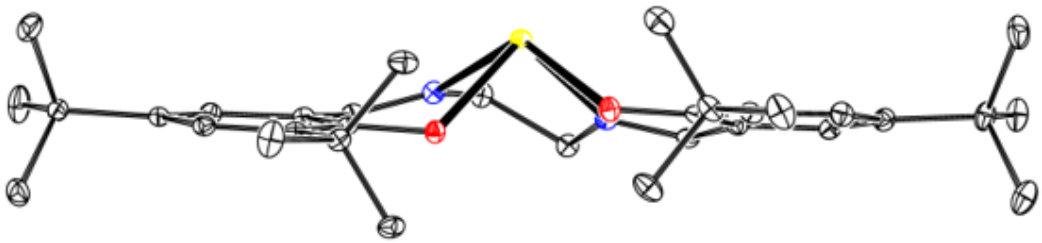

Figure 7: The coordination environment of the tin(II) atom in the complex **5** viewed along the plane of the ligand. Thermal displacement elipsoids were plotted at the 30 % probability level. All hydrogen atoms were omitted for the sake of clarity. Applied colours: C – black, N – blue, O – red, Sn – yellow.

3.2.5 [Sn(Salen)(Ph)Cl] complex **6**

Attempts were made to expand the general procedures to the synthesis of **6** with modified axial ligands. Preliminary results were positive, but upon detailed analysis, we found that the complex disproportionates to [Sn(Salen)Cl_2] and polymeric – [Sn(salenH)$(Ph)_2]_n$- (Scheme 7).

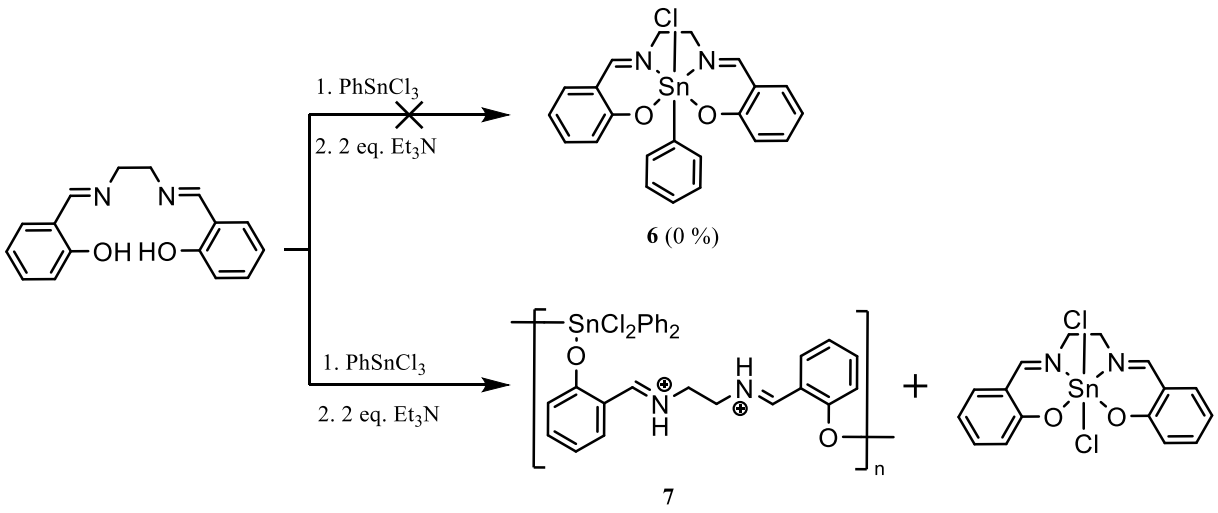

Scheme 7: Attempted synthesis of [Sn(Salen)(Ph)Cl].

The crystal of the THF-solvated coordination polymer **7** · 2 THF (Figure 8) was obtained by allowing THF vapors diffuse into a mixture obtained by reacting phenyltin trichloride with *N*,*N*′-bis(salicylidene)ethylenediamine in the presence of Et_3N in acetonitrile. Notably, the colorless needles of **7** · 2 THF were accompanied by colorless plates of [Sn(salen)Cl_2] complex, that was studied previously.[36]. The stannic coordination polymer **7** crystallized in the triclinic system with the space group *P*−1 as a THF solvate **7** · 2 THF with a single repeating unit and 2 THF molecules in the unit cell. The tin(IV) central atom finds itself in a special position with the associated Wyckoff letter *h* (site symmetry C_i) in a deformed octahedral coordination environment with all 3 pairs of donor atoms (2 chloride anions, 2 carbon donor atoms and 2 oxygen donor atoms) coordinated in *trans* configuration. The polymer chains propagate in the [1 1 0] direction (Figure 9). Due to the conformation of the protonated *N*,*N*′-bis(salicylidene)ethylenediamine ligand, the hydrogen atom H1 of the iminium group is located in the vicinity of the oxygen donor atom O1 (symmetry operation code of the acceptor *x*,*y*,*z*, N1···O1 = 2.608(3) Å, H1···O1 = 1.89 Å, N1-H1···O1 = 137°), as well as the dichloro ligand chlorine atom Cl1 (symmetry operation code of the acceptor 1 − x, 1 − y, 1 − z, N1···O1 = 3.338(2) Å, H1···O1 = 2.64 Å, N1-H1···O1 = 136°) The graph set[45] descriptors of the corresponding intramolecular hydrogen bonds are S(6) and S(8) respectively.

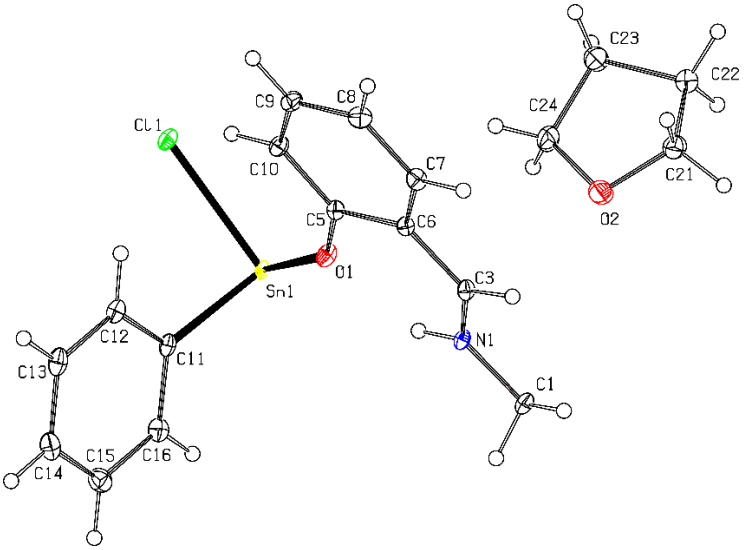

Figure 8: The contents of the asymmetric unit in the crystal structure of **7** · 2 THF with the corresponding atom numbering scheme. Thermal displacement elipsoids were plotted at the 30 % probability level. Applied colours: C – black, H – black contour, Cl – green, N – blue, O – red, Sn – yellow.

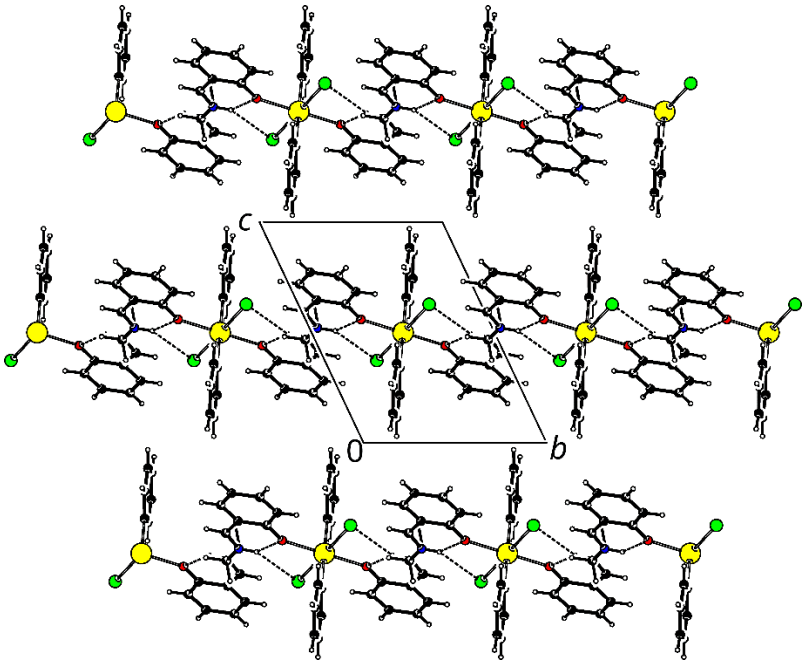

Figure 9: Sections of adjacent infinite chains of the coordination polymer **7** in the crystal structure of **7** · 2 THF viewed along the axis *a*. The unit cell is outlined by a solid line. Potential hydrogen bonds are outlined by dashed lines. The solvating THF molecules were omitted from the plot for the sake of clarity. Applied colours: C – black, H – black contour, Cl – green, N – blue, O – red, Sn – yellow.

3.3 Testing of synthesized complexes

3.3.1 Catalytic testing

The synthesized complexes 1-5 were tested in imine hydrogenation reaction, using *N*-tert-butyl-benzylimine (Scheme 8) as the model substrate. *N*-tert-butyl-benzylimine is frequently employed in FLP mediated imine hydrogenation reactions and hence allows rapid comparison to related systems.[14]

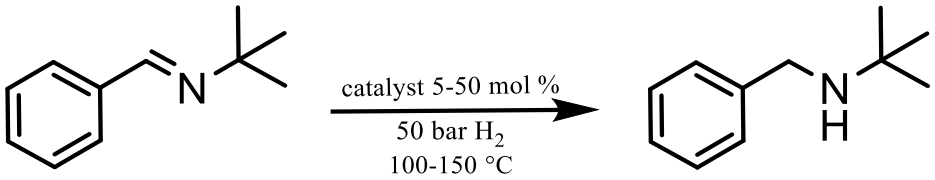

Scheme 8: Scheme of the catalytic tests.

The prepared complexes were tested under varying reaction conditions. The initial reaction conditions (50 bar of H_2, 150 °C, 5 mol% catalyst loading, 17 hours) in dry toluene (4 ml) were set based on the benchmark catalyst [Sn(salen)Cl_2], which yields the product at 27 % under these conditions.[36]

We hypothesized that [Sn(salen)Cl_2] under such conditions is limited by solubility in non-polar solvents. The addition of ^{t}Bu group to the classical *N*,*N*'-bis(salicylidene)ethylenediamine ligand improved the solubility of the final complexes. Accordingly, complex **1** acts as a very efficient catalyst yielding the desired product in 90 % yield (Table 1, entry 1). The high yield confirms the hypothesis and improves the catalytic performance, as previously the yields above 90 % were only obtained at harsher conditions, particularly at 180 °C. However, decreasing the temperature from 150 °C to120 °C using complex **1** as the catalyst completely stopped the reaction (Table 1, entry 2). Under such conditions the chloride-ligand is presumably too poor of a leaving group to facilitate formation of a free vacant site on the tin center and H_2 activation.

Therefore, we tested complexes containing triflate group(s) (**2** and **3**). The triflate is only weakly coordinating, thus making it a much more suitable leaving group than the chloride at lower temperatures. However, neither complex **2** nor complex **3** catalyzed the desired hydrogenation reaction at 120 °C (Table 1, entries 3 and 4) and showed no conversion of

the imine starting material to the amine product, indicating that chloride dissociation is not the only limiting factor of the reaction.

To avoid the imine substrate and produced amine binding to the catalyst, the acidity of the Lewis acid was decreased by the use of tin(II) instead of tin(IV). We tested the complex **5** at 150 °C (Table 1, entry 5) to see if **5** can mediate imine hydrogenation. However, the complex **5** failed to yield the desired amine product (Table 1, entry 5). The inability of tin(II) complexes to catalyze imine hydrogenation may be caused by the fact that the tin(II) center lies above the plane of the ligand (Figure 7), thus forming a classical Lewis adduct with the imine substrate and quenching the complex's reactivity. It could also be caused by the low acidity of the tin (II) species, hindering the activation of dihydrogen. Further catalytic tests, H_2 activation studies and effect of additional reaction base should be performed to answer these hypotheses.

Table 1: Preliminary catalytic results.

Entry	Complex	Temperature [°C]	Yield [%]
1	1	150	90
2	1	120	0
3	2	120	0
4	3	120	0
5	5	150	0

4. Conclusion

In this thesis, a series of hexa- and tetra-coordinated complexes of tin(IV) and tin(II) with Schiff base ligands was synthesized. The structure of the complexes was analyzed by NMR measurements, and **1** and **5** were also analyzed by sXRD. Their ability to catalyze imine hydrogenations was tested under various conditions. The dichloro complex **1** was able to mediate the hydrogenation at 150 °C in toluene with excellent yield. However, it was not able to mediate the hydrogenation at lower temperatures. The triflate containing complexes **2** and **3** were not able to mediate the reaction at 120 °C. The tetra-coordinated

tin(II) complex **5** also did not catalyze the reaction. The results show that the divalent tin cation is not acidic enough to act as a suitable LA component of the FLP. Future studies should consider modifying complex **1** with other, better leaving axial substituents, assess the ability of the complexes in combination with the imine substrate to act as H_2 activation FLP catalysts and consider the suitability of the non-polar media applied in the reactions. The effect of produced amine binding to the catalyst should also be assessed.

5. Experimental

The solvents and chemicals were either available in the laboratory or were purchased from commercial suppliers in the highest available purity. Solvents were dried using a solvent purification system, or by storing on molecular sieves and degassing. Glassware was dried in an oven at 180 °C overnight before using.

All synthesized complexes were analyzed using ^{1}H, ^{13}C and ^{119}Sn NMR spectroscopy (except complexes **2** and **5**, which were not analyzed by ^{119}Sn NMR). In addition, the triflate complexes were also analyzed using ^{19}F NMR spectroscopy Solvents used for NMR spectroscopy measurements were DMSO-d6 or $CDCl_3$. NMR measurements were performed on Bruker Avance NEO (400 MHz) at room temperature. Chemical shifts for ^{1}H are given in δ relative to the tetramethylsilane (TMS) and are referenced to the residual protium in the NMR solvent (DMSO-d6: δ = 2.50 ppm, $CDCl_3$: δ = 7,26 ppm). Chemical shifts for ^{13}C are given in δ relative to the TMS and are referenced to the carbon resonances in the solvent (DMSO-d6: δ = 39.5 ppm, $CDCl_3$: δ = 77.0 ppm). Also, where crystals of sufficient quality could be obtained, single crystal X-Ray diffraction (sXRD) patterns were measured to determine the geometry of the complexes.

5.1 sXRD measurements

The crystals selected for X-ray diffraction analysis were grown by a slow diffusion of excess hexane into a DCM (0.5 ml) solution of complex **1** (10 mg) in an NMR tube, by cooling a heptane solution of **5** or from THF (**7**).

The diffraction data were acquired on a Bruker D8 VENTURE Kappa Duo diffractometer with a PHOTONIII detector, an Incoatec IμS microfocus sealed tube source

and a Cryostream Cooler (Oxford Cryostreams). The diffraction data were collected at 120(2) K using monochromated MoK_α radiation (λ = 0,71073 Å). The acquired data were reduced using the software of the diffratometer (SAINT[46]) and corrected for absorption using methods incorporated in the diffractometer software (SADABS[47]).

The crystal structures were elucidated by intrinsic phasing methods using the program SHELXT[48] version 2018 and refined by weighted full-matrix least-squares against F^2 using the program SHELXL-2019.[49] All non-hydrogen atoms were refined by anisotropic displacement parameters. The corresponding Fourier maxima were located for all hydrogen atoms, which were then refined isotropically. The hydrogen atoms of the CH_n groups were refined as riding atoms with $U_{iso}(H) = 1.2\ U_{eq}(C)$ in the case of CH and CH_2 groups, or with $U_{iso}(H) = 1.5\ U_{eq}(C)$ in the case of CH_3 groups. The single symmetry-independent iminium group hydrogen atom in the molecule of the coordination polymer **7** was fixated in the position of the corresponding difference electron density map maximum under the rigid-body movement assumption with $U_{iso}(H) = 1.2\ U_{eq}(N)$. After the final cycle of refinement of the structure of the solvated coordination polymer **7** · 2 THF, the corresponding residual difference electron density map contained the maximum of 2.04 e · $Å^{-3}$ nearby (1.09 Å) the carbon atom C10 of the phenylene moiety of the bridging ligand, whereas the residual difference electron density map minimum of −0.99 e · $Å^{-3}$ was located in the vicinity (0.82 Å) of the tin atom Sn1.

In the crystal structure of the stannous complex **5**, a solvating molecule was found extensively disordered around the crystallographic two-fold rotation axis in a solvent accessible void. Even though carbon atoms of a toluene molecule could be placed into the difference electron density maxima and refined, the disorder of the molecule could not be modelled with a satisfactory result. Therefore, the contribution of the disordered solvent molecule to the overall scattering was removed using the program suite PLATON/SQUEEZE.[50] In total, 217 electrons were removed across four structural voids in one unit cell. The theoretical value for residual toluene likely accompanying the stannous complex as a reaction solvent from previous synthetic steps is 200 electrons, whereas the theoretical value for heptane from the crystallization mixture is 232 electrons (space group *C*2/*c*, *Z* = 4). NMR analysis of the complex indicates that both toluene and heptane may have co-crystallized in the structural voids.

Selected structure solution and refinement parameters are listed in Table 2. All geometric parameters and graphics were calculated and plotted using PLATON

program.[51,52] The provided values were rounded with respect to their estimated standard deviations.

Table 2: Crystallographic data and structure refinement for [Sn(3-^{t}Bu-salen)Cl_2] [Sn(3,5-di-^{t}Bu-salen)] and [Sn(Salen)Cl_2] with –[Sn(SalenH)$(Ph)_2]_n$-.

Structure code	[Sn(3-^{t}Bu-salen)Cl_2]	Solvated [Sn(3,5-di-^{t}Bu-salen)]	-[Sn(SalenH)$(Ph)_2]_n$- · 2 THF
Empirical formula	$C_{24}H_{30}N_2O_2Sn$	$C_{32}H_{46}N_2O_2Sn$	$C_{28}H_{26}N_2O_2Sn$
Formula weight [g · mol^{-1}]	568.09	609.42	756.30
Crystal system	Monoclinic	Monoclinic	Triclinic
Space group	$P2_1/c$	$C2/c$	$P\bar{1}$
a [Å]	23.1845(5)	21.3360(8)	8.9343(7)
b [Å]	7.84850(10)	10.2618(3)	9.3464(7)
c [Å]	13.4398(3)	32.1586(18)	11.6618(10)
α [°]	90	90	112.483(3)
β [°]	94.1780(10)	108.252(2)	92.478(3)
γ [°]	90	90	111.035(3)
V [Å^3]	2439.05(8)	6686.7(5)	821.23(12)
Z	4	8	1
F(000)	1152	2744	388
Calculated density [g · cm^{-3}]	1,547	1.302	1.529
μ(Mo K$_\alpha$) [mm^{-1}]	1.290	0.796	0.983
Crystal size [mm]	0.140 · 0.074 · 0.027	0.265 · 0.135 · 0.082	0.177 · 0.087 · 0.034
θ range [°]	2.634 – 28.324	2.424 – 28.3024	1.933 – 28.378

Collected diffractions	71230	103355	50160
Independent diffractions	6074	8361	4108
Observed[a] diffractions	5736	7889	4044
R_{int}[b] [%]	5.24	3.06	5.63
Number of parameters	286	346	205
R, wR[c] (observed) [%]	2.65, 4.85	1.93, 4.49	0.0280, 0.0698
R, wR[c] (all data) [%]	2.93, 4,94	2.12, 4.57	0.0288, 0.0703
Goodness of fit[d]	1.136	1.064	1.109
$\Delta\rho_{max}$ and $\Delta\rho_{min}$ ($e \cdot Å^{-3}$)	0.574, −0.896	0.381, −0.345	2.043, −0.985
Weighting scheme	w = $1/[\sigma^2 (F_o^2) + (aF)^2 + bP]$; where $P = (F_o^2 + 2F_c^2) / 3$.		
	a = 0.0085	a = 0.0151	a = 0.0372
	b = 3.1597	b = 8.5001	b = 0.7724

[a] $| > 2\sigma (|)$

[b] $R_{int} = \sum |F_o^2 - F_{o,mean}^2| / \sum F_o^2$

[c] $R(F) = \sum | |F_o| - |F_c| | / \sum |F_o|$; $wR(F^2) = [\sum (w(F_o^2 - F_c^2)^2) / \sum w(F_o^2)^2]^{1/2}$

[d] $S = [\sum (w(F_o^2 - F_c^2)^2) / (N_{diffrns} - N_{par})]^{1/2}$

General synthesis procedure of salen, 3-tert-butyl-salen and 3,5-di-tert-butyl-salen

The general synthetic procedure for all ligands followed literature.[39] 1 equivalent of ethylenediamine with 2 equivalents of the corresponding salicylaldehyde were dissolved together in EtOH and refluxed. The course of the reactions was monitored with NMR measurements. The solutions were cooled down, filtered and washed with cold EtOH. The solid products were dried in air.

Salen

40 mmol (4.21 ml) of salicylaldehyde were used with 20 mmol (1.33 ml) of ethylenediamine and 150 ml of EtOH. The mixture was refluxed for 2 hours. The product was isolated as yellow crystals in 95 % (5.07 g) yield. ^{1}H NMR (400 MHz, $CDCl_3$) δ 13.20 (s, 2H), 8.36 (s, 2H), 7.34 – 7.27 (m, 2H), 7.23 (dd, J = 7.6, 2.1 Hz, 2H), 6.94 (d, J = 8.4 Hz, 2H), 6.86 (t, J = 7.5 Hz, 2H), 3.94 (s, 4H). ^{13}C NMR (101 MHz, $CDCl_3$) δ 166.5, 161.0, 132.4, 131.5, 118.7, 118.7, 117.0, 59.8.

3-tert-butyl-salen

50 mmol (8,56 ml) of 3-tert-butyl-salicylaldehyde were used with 25 mmol (1,67 ml) of ethylenediamine and 200 ml of EtOH. The mixture was refluxed for 2 hours. The product was isolated as yellow dust in 98 % (9,30 g) yield. ^{1}H NMR (400 MHz, DMSO) δ 13.09 (s, 2H), 8.58 (s, 2H), 7.45 – 7.31 (m, 4H), 6.79 (d, J = 8.6 Hz, 2H), 3.90 (s, 4H), 3.32 (s, 14H). ^{13}C NMR (101 MHz, DMSO) δ 167.7, 158.7, 141.2, 130.0, 128.4, 118.4, 116.4, 59.5, 34.2, 31.7.

3,5-di-tert-butyl-salen

50 mmol (11,72 g) of 3,5-di-tert-butyl-salicylaldehyde were used with 25 mmol (1,67 ml) of ethylenediamine and 200 ml of EtOH. The mixture was refuxed for 2 hours. The product was isolated as yellow powder in 92 % (11,40 g) yield. ^{1}H NMR (400 MHz, CDCl 3) δ 13.63 (s, 2H), 8.39 (s, 2H), 7.36 (d, J = 2.5 Hz, 2H), 7.06 (d, J = 2.5 Hz, 2H), 3.92 (s, 4H), 1.43 (s, 18H), 1.28 (s, 18H). ^{13}C NMR (101 MHz, $CDCl_3$) δ 167.6, 158.0, 140.1, 136.6, 127.0, 126.1, 117.8, 59.6, 35.0, 34.1, 29.4

.

General synthesis procedure of [Sn(3-^{t}Bu-salen)Cl_2] complex **1**

Reactions were performed under nitrogen atmosphere using a Schlenk line apparatus. Solvents and glassware were dried according to the general procedure mentioned above. The starting ligand was dried in vacuum for 1 hour before synthesis. The ligand was dissolved in DCM and $SnCl_4$ was added to the flask through septum with a syringe that had been flushed with nitrogen. After 5 minutes of stirring, dry Et_3N was added to the solution through septum with a syringe that had also been flushed with nitrogen. The solution was stirred overnight and the solvent was then evaporated. The solid was washed with EtOH and the solvent was then filtered out via cannula. Dry heptane was then added to the solid and boiled while stirring. The heptane was then filtered out via cannula while hot. And the product was dried in vacuum and stored under nitrogen atmosphere.

Complex **1**

5 mmol (1,90 g) of 3-tert-butyl-salen ligand was dissolved in 35 ml of DCM. 5 mmol (588 µl) of $SnCl_4$ was added to the solution. The solution was stirred overnight. The solvent was then evaporated and 50 ml of EtOH was added to the solid. EtOH was then filtered out via cannula. 60 ml of heptane was added and the solution was heated to 105 °C. The solution was then filtered through a filter paper while hot, and the solid product was dried in vacuum. The yellow product was obtained in 59 % (1,67 g) yield. ^{1}H NMR (400 MHz, DMSO) δ 8.80 (s, 2H), 7.60 (dd, J = 8.8, 2.8 Hz, 2H), 7.49 (d, J = 2.8 Hz, 2H), 6.86 (d, J = 8.8 Hz, 2H), 4.16 (s, 4H), 1.29 (s, 19H). ^{13}C NMR (101 MHz, DMSO) δ 172.7, 163.3, 141.3, 134.8, 132.9, 122.7, 117.3, 51.7, 34.2, 31.5. ^{119}Sn NMR (149 MHz, DMSO) δ -600.

General synthesis procedure of triflate containing complexes

Reactions were performed in a glovebox filled with nitrogen atmosphere. Solvents and glassware were dried according to the general procedure mentioned above. The complex **1** was dried under vacuum for 1 hour before the synthesis. The complex **1** was dissolved in DCM and 1 eq. of AgOTf was added in case of complex **2** and 2 eq. AgOTf was added in

case of complex **3**. The flasks were covered in aluminum foil and the reaction mixtures were stirred for 96 hours. The course of reactions was monitored through NMR measurements. The produced complexes were filtered to another flask via cannula to separate them from the precipitated AgCl side product. The solvent was evaporated and the yellow solids were dried in vacuum. Products were stored under nitrogen atmosphere.

Complex **2**

0.6 mmol (340 mg) of complex **1** was dissolved in 15 ml of DCM. 0.6 mmol (154 mg) of AgOTf was added to the solution. The solution was stirred at room temperature for 96 hours. Solution was then filtered via cannula to a new flask and the liquid was evaporated, yielding a pale yellow solid. ^{1}H NMR (400 MHz, $CDCl_3$) δ 8.41 (s, 2H), 7.62 (dd, J = 8.9, 2.6 Hz, 2H), 7.22 (d, J = 2.6 Hz, 2H), 7.10 (d, J = 8.9 Hz, 2H), 4.39 – 4.15 (m, 4H), 1.30 (s, 18H). ^{13}C NMR (101 MHz, $CDCl_3$) δ 172.8, 164.2, 142.6, 136.3, 131.9, 123.4, 116.3, 51.6, 34.0, 31.3, 31.1. ^{19}F NMR (376 MHz, $CDCl_3$) δ -77.82.

Complex **3**

0,35 mmol (200 mg) of complex **1** was dissolved in 15 ml of DCM. 0,7 mmol (180 mg) of AgOTf was added to the solution. The solution was stirred at room temperature for 96 hours. Solution was then filtered via cannula to a new flask and the liquid was evaporated, yielding a dark yellow solid in 39 % (110 mg) yield. ^{1}H NMR (400 MHz, $CDCl_3$) δ 8.54 (s, 1H), 7.68 (dd, J = 8.9, 2.6 Hz, 1H), 7.27 (s, 1H), 7.15 (d, J = 8.9 Hz, 1H), 4.34 (s, 2H), 1.32 (s, 9H). ^{13}C NMR (101 MHz, $CDCl_3$) δ 174.8, 164.3, 143.5, 137.2, 132.1, 123.2, 116.1, 53.4, 51.0, 34.1, 31.2, 31.0. ^{19}F NMR (376 MHz, $CDCl_3$) δ -77.39. ^{119}Sn NMR (149 MHz, $CDCl_3$) δ -650.20.

General synthesis procedure of tin(II) complexes

Reactions were perfomed in a glovebox filled with nitrogen atmosphere. Solvents and glassware were dried according to the general procedure. The ligand was dried in vacuum for 1 hour before synthesis. $[(Me_3Si)N]_2$ was then added to the flask and the chemicals were dissolved in toluene. The reaction mixtures were stirred for 4 hours, giving a yellow

precipitate. The solvent was then filtered out via cannula and the yellow solids were washed with toluene and pentane in the case of complex **4** and with toluene in the case of complex **5**. The solvents were then filtered out via cannula and the yellow solids were dried in vacuum and stored under nitrogen atmosphere.

Complex **4**

0,7 mmol (0,3 g) of 3-tert-butyl-salen and 0,9 mmol (0,39 g) of $[(Me_3Si)N]_2Sn$ were added to a Schlenk flask. The chemicals were dissolved in dry toluene (5 ml). The reaction mixture was stirred for 4 hours at room temperature, giving a yellow precipitate. The solvent was filtered out via cannula and the yellow solid was washed with dry toluene (3 ml) and pentane (10 ml). The solvents were filtered out via cannula and the yellow product was dried under vacuum. ^{1}H NMR (400 MHz, DMSO) δ 8.40 (s, 2H), 7.34 (dd, J = 8.8, 2.8 Hz, 2H), 7.20 (d, J = 2.8 Hz, 2H), 6.65 (d, J = 8.8 Hz, 2H), 4.07 (d, J = 6.6 Hz, 2H), 3.68 (d, J = 7.3 Hz, 2H), 2.51 (s, 18H). ^{13}C NMR (101 MHz, $CDCl_3$) δ 167.1, 166.9, 164.1, 138.5, 132.7, 129.7, 129.5, 127.9, 123.6, 118.9, 116.4, 60.0, 55.7, 33.7, 31.4. ^{119}Sn NMR (149 MHz, $CDCl_3$) δ -544.

Complex **5**

2 mmol (1 g) od 3,5-di-tert-butyl-salen and 2.4 mmol (1.04 g) of $[(Me_3Si)N]_2Sn$ were added to a Schlenk flask. The chemicals were dissolved in dry toluene (15 ml). The reaction mixture was stirred for 4 hours at room temperature, yielding a yellow precipitate. The solvent was filtered out via cannula and the solid was washed with dry boiling heptane (3 ml). The heptane was then filtered out via cannula while hot, and the yellow product was dried under vacuum. ^{1}H NMR (400 MHz, $CDCl_3$) δ 8.14 (s, 2H), 7.43 (d, J = 2.8 Hz, 2H), 6.91 (d, J = 2.6 Hz, 2H), 3.92 (s, 2H), 3.70 (d, J = 5.4 Hz, 2H), 1.49 (s, 18H), 1.29 (s, 19H). ^{13}C NMR (101 MHz, $CDCl_3$) δ 167.6, 142.2, 137.2, 129.6, 127.5, 119.7, 55.7, 35.4, 33.9, 31.4, 29.8.

Crystallographic data

Table 3: Selected angles and bond lengths of [Sn(3-tBu-salen)Cl_2.

bond	Value [Å]	Angle	Value [°]	Torsion	Value [°]
Sn1-Cl1	2.4036(7)	Cl1-Sn1-CL2	175.68(2)	Cl1-Sn1-O1-C5	128.57(13)
Sn1-Cl2	2.4250(6)	Cl1-Sn1-O1	89.69(4)	Cl2-Sn1-O1-C5	−54.89(13)
Sn1-O1	2.0173(14)	Cl1-Sn1-O2	89.92(4)	O2-Sn1-O1-C5	−141.61(13)
Sn1-O2	2.0055(14)	Cl1-Sn1-N1	93.18(5)	N1-Sn1-O1-C5	35.38(14)
Sn1-N1	2.1525(15)	Cl1-Sn1-N2	90.53(5)	Cl1-Sn1-O2-C11	−59.45(13)
Sn1-N2	2.1723(16)	Cl2-Sn1-O1	87.71(4)	Cl2-Sn1-O2-C11	124.00(13)
O1-C5	1.340(2)	Cl2-Sn1-O2	87.48(4)	O1-Sn1-O2-C11	−149.10(13)
O2-C11	1.341(2)	Cl2-Sn1-N1	90.21(5)	N2-Sn1-O2-C11	31.08(14)
N1-C1	1.465(2)	Cl2-Sn1-N2	92.85(5)	Cl1-Sn1-N1-C1	74.15(12)
N1-C3	1.284(2)	O1-Sn1-O2	105.95(6)	Cl1-Sn1-N1-C1	−113.50(15)
N2-C2	1.469(2)	O1-Sn1-N1	88.53(6)	Cl1-Sn1-N1-C3	−108.54(12)
N2-C4	1.284(2)	O1-Sn1-N2	165.48(6)	Cl2-Sn1-N1-C1	63.81(15)
C1-C2	1.522(2)	O2-Sn1-N1	165.22(6)	Cl2-Sn1-N1-C3	163.76(12)
C3-C6	1.443(2)	O2-Sn1-N2	88.57(6)	O1-Sn1-N1-C1	−23.89(15)
C4-C12	1.449(3)	N1-Sn1-N2	76.96(6)	O1-Sn1-N1-C3	−15.66(12)
C5-C6	1.419(3)	Sn1-O1-C5	121.97(11)	N2-Sn1-N1-C1	156.69(16)
C5-C10	1.399(2)	Sn1-O2-C11	123.79(12)	N2-Sn1-N1-C3	−104.10(12)
C6-C7	1.414(3)	Sn1-N1-C1	114.32(11)	Cl1-Sn1-N2-C2	72.34(15)
C7-C8	1:381(2)	Sn1-N1-C3	123.12(12)	Cl1-Sn1-N2-C4	78.59(12)
C8-C9	1.405(3)	C1-N1-C3	122.10(15)	Cl2-Sn1-N2-C2	−104.10(12)
C8-C17	1.531(3)	Sn1-N2-C2	114.16(11)	Cl2-Sn1-N2-C4	77.34(15)

C9-C10	1.378(3)	Sn1-N2-C4	123.70(12	O2-Sn1-N2-C2	78.59(12)
C11-C12	1.415(2)	C2-N2-C4	122.05(15)	O2-Sn1-N2-C4	−104.97(15)
C11-C16	1.394(3)	N1-C1-C2	108.31(15)	N1-Sn1-N2-C2	166.00(13)
C12-C13	1.414(2)	N2-C2-C1	108.71(14)	N1-Sn1-N2-C4	165.48(16)
C13-C14	1.388(3)	N1-C3-C6	125.51(16)	Sn1-O1-C5-C6	−33.2(2)
C14-C15	1.400(3)	N2-C4-C12	125.64(15)	Sn1-O1-C5-C10	149.97(13)
C14-C21	1.532(3)	O1-C5-C6	124.83(16)	Sn1-O2-C11-C12	−31.2(2)
C15-C16	1.380(3)	C6-C5-C10	117.77(16)	Sn1-O2-C11-C16	151.46(14)

Table 4: Selected bond lengths and angles of [Sn(3,5-di-tBu-salen)].

bond	Value [Å]	angle	Value [°]	torsion	Value [°]
Sn1-O1	2.0980(10)	O1-Sn1-O2	78.91	O2-Sn1-O1-C5	166.37(10)
Sn1-O2	2.1360(11)	O1-Sn1-N1	75.11(4)	N1-Sn1-O1-C5	-57.33(9)
Sn1-N1	2.3776(11)	O1-Sn1-N2	105.17(4)	N2-Sn1-O1-C5	-119.58(9)
Sn1-N2	1.4486(17)	O2-Sn1-N1	129.51(4)	O1-Sn1-O2-C11	157.35(10)
O1-C5	1.3799(18)	O2-Sn1-N2	77.88(4)	N1-Sn1-O2-C11	97.42(11)
O2-C11	1.533717)	N1-Sn1-N2	68.46(4)	N2-Sn1-O2-C11	49.01(10)
N1-C1	1.3742(17)	Sn1-O1-C5	122.87(8)	O1-Sn1-N1-C1	-147.21(9)
N1-C3	1.5340(19)	Sn1-O2-C11	126.75(8)	O1-Sn1-N1-C3	34.99(10)
N2-C2	1.4717(15)	Sn1-N1-C3	124.72(9)	O2-Sn1-N1-C1	-85.71(9)
N2-C4	1.3129(16)	C1-N1-C3	122.53(10)	O2-Sn1-N1-C3	96.49(11)
C1-C2	1.2842(16)	Sn1-N2-C2	119.93(7)	N2-Sn1-N1-C1	-33.88(8)
C3-C6	1.4166(17)	Sn1-N2-C4	122.99(8)	N2-Sn1-N1-C3	148.32(12)
C4-C12	1.4035(17)	C2-N2-C4	116.93(10)	O1-Sn1-N2-C2	77.02(10)

C5-C6	1.4179(18)	N1-C1-C2	107.62(10)	O1-Sn1-N2-C4	-107.64(11)
C5-C10	1.407(2)	N2-C2-C1	109.87(10)	O2-Sn1-N2-C2	151.83(10)
C6-C7	1.4051(18)	N1-C3-C6	123.71(11)	O2-Sn1-N2-C4	-32.82(10)
C7-C8	1.4511(17)	N2-C4-C12	126.69(12)	N1-Sn1-N2-C2	10.17(9)
C8-C9	1.5230(18)	O1-C5-C6	119.76(11)	N1-Sn1-N2-C4	-174.48(12)
C8-C17	1.4274(19)	O1-C5-C10	122.04(12)	Sn1-O1-C5-C6	53.57(15)
C9-C10	1.5311(18)	C6-C5-C10	118.16(11)	Sn1-O1-C5-C10	-128.65(11)
C10-C25	1.4292(17)	C3-C6-C5	121.44(11)	Sn1-O2-C11-C12	-40.42(16)
C11-C12	1.527(2)	C3-C6-C7	117.74(11)	Sn1-O2-C11-C16	141.80(10)
C11-C16	1.4292(17)	C5-C6-C7	120.79(12)	Sn1-N1-C1-C2	52.04(11)
C12-C13	1.2747(17)	C6-C7-C8	121.78(11)	C3-N1-C1-C2	-130.10(13)
C13-C14	1.4545(18)	C7-C8-C9	116.34(11)	Sn1-N1-C3-C6	-5.82(18)
C14-C15	1.4051(18)	C7-C8-C17	124.45(11)	C1-N1-C3-C6	-5.82(18)
C14-C21	1.3821(18)	C9-C8-C17	119.20(11)	Sn1-N2-C2-C1	-5.82(18)
C15-C16	1.4054(18)	C8-C9-C10	124.98(12)	N1-C1-C2-N2	-41.22(14)
C16-C29	1.3811(19)	O2-C11-C12	121.75(11)		

Literature

(1) Lowry, T. M. Valence and the Structure of Atoms and Molecules. By Prof. G. N. Lewis. Pp. 172. American Chemical Monograph Series. New York: The Chemical Catalog Co., Inc., 1923. *J. Soc. Chem. Ind.* **1924**, *43* (1), 17–17. https://doi.org/10.1002/jctb.5000430107.

(2) *Lewis Acid and Base - an overview | ScienceDirect Topics*. https://www.sciencedirect.com/topics/engineering/lewis-acid-and-base.

(3) Scott, D. J.; Fuchter, M. J.; Ashley, A. E. Designing Effective 'Frustrated Lewis Pair' Hydrogenation Catalysts. *Chem. Soc. Rev.* **2017**, *46* (19), 5689–5700. https://doi.org/10.1039/C7CS00154A.

(4) Weicker, S. A.; Stephan, D. W. Main Group Lewis Acids in Frustrated Lewis Pair Chemistry: Beyond Electrophilic Boranes. *Bull. Chem. Soc. Jpn.* **2015**, *88* (8), 1003–1016. https://doi.org/10.1246/bcsj.20150131.

(5) Guo, Y.; Lian, X.; Zhang, H.; Zhang, X.; Chen, J.; Chen, C.; Lan, X.; Shao, Y. Systematic Assessment of the Catalytic Reactivity of Frustrated Lewis Pairs in C-H Bond Activation. *Molecules* **2023**, *29* (1), 24. https://doi.org/10.3390/molecules29010024.

(6) Rocchigiani, L. Experimental Insights into the Structure and Reactivity of Frustrated Lewis Pairs. *Isr. J. Chem.* **2015**, *55* (2), 134–149. https://doi.org/10.1002/ijch.201400139.

(7) Ménard, G.; Tran, L.; Stephan, D. W. Activation of H2 Using P/Al Based Frustrated Lewis Pairs and Reactions with Olefins. *Dalton Trans.* **2013**, *42* (37), 13685–13691. https://doi.org/10.1039/C3DT51739J.

(8) Farrell, J. M.; Hatnean, J. A.; Stephan, D. W. Activation of Hydrogen and Hydrogenation Catalysis by a Borenium Cation. *J. Am. Chem. Soc.* **2012**, *134* (38), 15728–15731. https://doi.org/10.1021/ja307995f.

(9) Welch, G. C.; Cabrera, L.; Chase, P. A.; Hollink, E.; Masuda, J. D.; Wei, P.; Stephan, D. W. Tuning Lewis Acidity Using the Reactivity of "Frustrated Lewis Pairs": Facile Formation of Phosphine-Boranes and Cationic Phosphonium-Boranes. *Dalton Trans.* **2007**, No. 31, 3407–3414. https://doi.org/10.1039/B704417H.

(10) Follet, E.; Mayer, P.; Stephenson, D. S.; Ofial, A. R.; Berionni, G. Reactivity-Tuning in Frustrated Lewis Pairs: Nucleophilicity and Lewis Basicity of Sterically Hindered Phosphines. *Chem. – Eur. J.* **2017**, *23* (31), 7422–7427. https://doi.org/10.1002/chem.201701080.

(11) Sapsford, J. S.; Csókás, D.; Scott, D. J.; Turnell-Ritson, R. C.; Piascik, A. D.; Pápai, I.; Ashley, A. E. Establishing the Role of Triflate Anions in H2 Activation by a Cationic Triorganotin(IV) Lewis Acid. *ACS Catal.* **2020**, *10* (14), 7573–7583. https://doi.org/10.1021/acscatal.0c02023.

(12) *Reversible, Metal-Free Hydrogen Activation*. https://doi.org/10.1126/science.1134230.

(13) Scott, D. J.; Simmons, T. R.; Lawrence, E. J.; Wildgoose, G. G.; Fuchter, M. J.; Ashley, A. E. Facile Protocol for Water-Tolerant "Frustrated Lewis Pair"-Catalyzed Hydrogenation. *ACS Catal.* **2015**, *5* (9), 5540–5544. https://doi.org/10.1021/acscatal.5b01417.

(14) Scott, D. J.; Phillips, N. A.; Sapsford, J. S.; Deacy, A. C.; Fuchter, M. J.; Ashley, A. E. Versatile Catalytic Hydrogenation Using A Simple Tin(IV) Lewis Acid. *Angew. Chem. Int. Ed.* **2016**, *55* (47), 14738–14742. https://doi.org/10.1002/anie.201606639.

(15) Mahdi, T.; Stephan, D. W. Enabling Catalytic Ketone Hydrogenation by Frustrated Lewis Pairs. *J. Am. Chem. Soc.* **2014**, *136* (45), 15809–15812. https://doi.org/10.1021/ja508829x.

(16) Scott, D. J.; Fuchter, M. J.; Ashley, A. E. Nonmetal Catalyzed Hydrogenation of Carbonyl Compounds. *J. Am. Chem. Soc.* **2014**, *136* (45), 15813–15816. https://doi.org/10.1021/ja5088979.

(17) Sapsford, J. S.; Scott, D. J.; Allcock, N. J.; Fuchter, M. J.; Tighe, C. J.; Ashley, A. E. Direct Reductive Amination of Carbonyl Compounds Catalyzed by a Moisture Tolerant Tin(IV) Lewis Acid. *Adv. Synth. Catal.* **2018**, *360* (6), 1066–1071. https://doi.org/10.1002/adsc.201701418.

(18) Ke, Z.; Li, Y.; Hou, C.; Liu, Y. Homogeneously Catalyzed Hydrogenation and Dehydrogenation Reactions – From a Mechanistic Point of View. *Phys. Sci. Rev.* **2018**, *3* (10). https://doi.org/10.1515/psr-2017-0038.

(19) Frey, G. D.; Lavallo, V.; Donnadieu, B.; Schoeller, W. W.; Bertrand, G. Facile Splitting of Hydrogen and Ammonia by Nucleophilic Activation at a Single Carbon Center. *Science* **2007**, *316* (5823), 439–441. https://doi.org/10.1126/science.1141474.

(20) Budzelaar, P. H. M.; Hughes, D. L.; Bochmann, M.; Macchioni, A.; Rocchigiani, L. H2 Activation by Zirconaziridinium Ions: σ-Bond Metathesis versus Frustrated Lewis Pair Reactivity. *Chem. Commun.* **2020**, *56* (17), 2542–2545. https://doi.org/10.1039/C9CC09466K.

(21) Waterman, R. σ-Bond Metathesis: A 30-Year Retrospective. *Organometallics* **2013**, *32* (24), 7249–7263. https://doi.org/10.1021/om400760k.

(22) Molander, G. A.; Romero, J. A. C. Lanthanocene Catalysts in Selective Organic Synthesis. *Chem. Rev.* **2002**, *102* (6), 2161–2186. https://doi.org/10.1021/cr010291+.

(23) Reznichenko, A. L.; Hultzsch, K. C. Catalytic σ-Bond Metathesis; Roesky, P. W., Ed.; Structure and Bonding; Springer Berlin Heidelberg: Berlin, Heidelberg, 2010; Vol. 137, pp 1–48. https://doi.org/10.1007/430_2010_17.

(24) Lewis Acid Transition-Metal-Catalyzed Hydrogen Activation: Structures, Mechanisms, and Reactivities | Request PDF. *ResearchGate* **2024**. https://doi.org/10.1002/chem.201903193.

(25) Hounjet, L. J.; Stephan, D. W. Hydrogenation by Frustrated Lewis Pairs: Main Group Alternatives to Transition Metal Catalysts? *Org. Process Res. Dev.* **2014**, *18* (3), 385–391. https://doi.org/10.1021/op400315m.

(26) Das, S.; Turnell-Ritson, R. C.; Dyson, P. J.; Corminboeuf, C. Design of Frustrated Lewis Pair Catalysts for Direct Hydrogenation of CO2. *Angew. Chem. Int. Ed.* **2022**, *61* (46), e202208987. https://doi.org/10.1002/anie.202208987.

(27) Daru, J.; Bakó, I.; Stirling, A.; Pápai, I. Mechanism of Heterolytic Hydrogen Splitting by Frustrated Lewis Pairs: Comparison of Static and Dynamic Models. *ACS Catal.* **2019**, *9* (7), 6049–6057. https://doi.org/10.1021/acscatal.9b01137.

(28) Rokob, T. A.; Hamza, A.; Stirling, A.; Soós, T.; Pápai, I. Turning Frustration into Bond Activation: A Theoretical Mechanistic Study on Heterolytic Hydrogen Splitting by Frustrated Lewis Pairs. *Angew. Chem. Int. Ed.* **2008**, *47* (13), 2435–2438. https://doi.org/10.1002/anie.200705586.

(29) Rokob, T. A.; Hamza, A.; Pápai, I. Rationalizing the Reactivity of Frustrated Lewis Pairs: Thermodynamics of H2 Activation and the Role of Acid−Base Properties. *J. Am. Chem. Soc.* **2009**, *131* (30), 10701–10710. https://doi.org/10.1021/ja903878z.

(30) Chase, P. A.; Jurca, T.; Stephan, D. W. Lewis Acid-Catalyzed Hydrogenation: B(C6F5)3-Mediated Reduction of Imines and Nitriles with H2. *Chem. Commun.* **2008**, No. 14, 1701–1703. https://doi.org/10.1039/B718598G.

(31) Rokob, T. A.; Hamza, A.; Stirling, A.; Pápai, I. On the Mechanism of B(C6F5)3-Catalyzed Direct Hydrogenation of Imines: Inherent and Thermally Induced Frustration. *J. Am. Chem. Soc.* **2009**, *131* (5), 2029–2036. https://doi.org/10.1021/ja809125r.

(32) Chen, D.; Klankermayer, J. Metal-Free Catalytic Hydrogenation of Imines with Tris(Perfluorophenyl)Borane. *Chem. Commun.* **2008**, No. 18, 2130–2131. https://doi.org/10.1039/B801806E.

(33) Chase, P. A.; Welch, G. C.; Jurca, T.; Stephan, D. W. Metal-Free Catalytic Hydrogenation. *Angew. Chem. Int. Ed.* **2007**, *46* (42), 8050–8053. https://doi.org/10.1002/anie.200702908.

(34) Farrell, J. M.; Posaratnanathan, R. T.; Stephan, D. W. A Family of N-Heterocyclic Carbene-Stabilized Borenium Ions for Metal-Free Imine Hydrogenation Catalysis. *Chem. Sci.* **2015**, *6* (3), 2010–2015. https://doi.org/10.1039/C4SC03675A.

(35) Paparakis, A.; Turnell-Ritson, R. C.; Sapsford, J. S.; Ashley, A. E.; Hulla, M. Tin-Catalyzed Reductive Coupling of Amines with CO2 and H2. *Catal. Sci. Technol.* **2023**, *13* (3), 637–644. https://doi.org/10.1039/D2CY01659A.

(36) Žáková, A.; Saha, P.; Paparakis, A.; Zábranský, M.; Gastelu, G.; Kukla, J.; Uranga, J. G.; Hulla, M. Hexacoordinated Tin Complexes Catalyse Imine Hydrogenation with H_2. *Chem. Commun.* **2024**, *60* (24), 3287–3290. https://doi.org/10.1039/D3CC05878F.

(37) Hansen, T. V.; Skattebøl, L. A High Yielding One-Pot Method for the Preparation of Salen Ligands. *Tetrahedron Lett.* **2005**, *46* (22), 3829–3830. https://doi.org/10.1016/j.tetlet.2005.03.193.

(38) (PDF) Molecular Structures of Sn(II) and Sn(IV) Compounds with Di-, Tri- and Tetramethylene Bridged Salen* Type Ligands. *ResearchGate* **2024**. https://doi.org/10.1515/mgmc-2014-0004.

(39) Milo, A.; Neumann, R. An Achiral Manganese Salen Catalyst Encapsulated in a Peptidic Phosphonate Homochiral Solid for the Enantioselective Formation of Diols by Consecutive Epoxidation and Hydration Reactions. *Chem. Commun.* **2011**, *47* (9), 2535–2537. https://doi.org/10.1039/C0CC04205F.

(40) *Ring-Opening Polymerization of Trimethylene Carbonate Using Aluminum(III) and Tin(IV) Salen Chloride Catalysts. Volume 38, Number 13, June 28, 2005, pp 5406−5410. | Request PDF*. https://www.researchgate.net/publication/231698791.

(41) Shaw, S.; White, J. D. Asymmetric Catalysis Using Chiral Salen–Metal Complexes: Recent Advances. *Chem. Rev.* **2019**, *119* (16), 9381–9426. https://doi.org/10.1021/acs.chemrev.9b00074.

(42) Yimthachote, S.; Chumsaeng, P.; Phomphrai, K. Complexity of Imine and Amine Schiff-Base Tin(II) Complexes: Drastic Differences of Amino and Pyridyl Side Arms. *Dalton Trans.* **2022**, *51* (2), 509–517. https://doi.org/10.1039/D1DT02997E.

(43) Kuchta, M. C.; Hahn, J. M.; Parkin, G. Divalent Tin and Lead Complexes of a Bulky Salen Ligand: The Syntheses and Structures of [SalenBut,Me]Sn and [SalenBut,Me]Pb. *J. Chem. Soc. Dalton Trans.* **1999**, No. 20, 3559–3563. https://doi.org/10.1039/A905490A.

(44) Westerhausen, M.; Schneiderbauer, S.; Kneifel, A. N.; Söltl, Y.; Mayer, P.; Nöth, H.; Zhong, Z.; Dijkstra, P. J.; Feijen, J. Organocalcium Compounds with Catalytic Activity for the Ring-Opening Polymerization of Lactones. *Eur. J. Inorg. Chem.* **2003**, *2003* (18), 3432–3439. https://doi.org/10.1002/ejic.200300286.

(45) Bernstein, J.; Davis, R. E.; Shimoni, L.; Chang, N.-L. Patterns in Hydrogen Bonding: Functionality and Graph Set Analysis in Crystals. *Angew. Chem. Int. Ed. Engl.* **1995**, *34* (15), 1555–1573. https://doi.org/10.1002/anie.199515551.

(46) Bruker, SAINT, V8.41, Bruker AXS Inc., Madison, Wisconsin, USA.

(47) Krause, L.; Herbst-Irmer, R.; Sheldrick, G. M.; Stalke, D. Comparison of Silver and Molybdenum Microfocus X-Ray Sources for Single-Crystal Structure Determination. *J. Appl. Crystallogr.* **2015**, *48* (1), 3–10. https://doi.org/10.1107/S1600576714022985.

(48) Sheldrick, G. M. SHELXT – Integrated Space-Group and Crystal-Structure Determination. *Acta Crystallogr. Sect. Found. Adv.* **2015**, *71* (1), 3–8. https://doi.org/10.1107/S2053273314026370.

(49) Sheldrick, G. M. Crystal Structure Refinement with SHELXL. *Acta Crystallogr. Sect. C Struct. Chem.* **2015**, *71* (1), 3–8. https://doi.org/10.1107/S2053229614024218.

(50) Spek, A. L. PLATON SQUEEZE: A Tool for the Calculation of the Disordered Solvent Contribution to the Calculated Structure Factors. *Acta Crystallogr. Sect. C Struct. Chem.* **2015**, *71* (1), 9–18. https://doi.org/10.1107/S2053229614024929.

(51) Spek, A. L. Single-Crystal Structure Validation with the Program PLATON. *J. Appl. Crystallogr.* **2003**, *36* (1), 7–13. https://doi.org/10.1107/S0021889802022112.

(52) (PDF) Structure Validation in Chemical Crystallography. *ResearchGate* **2025**. https://doi.org/10.1107/S090744490804362X.